nature cell biology

LncRNA *NBR2* engages a metabolic checkpoint by regulating AMPK under energy stress

Xiaowen Liu[1,8], Zhen-Dong Xiao[1,8], Leng Han[2], Jiexin Zhang[3], Szu-Wei Lee[4,5], Wenqi Wang[1], Hyemin Lee[1], Li Zhuang[1], Junjie Chen[1,5], Hui-Kuan Lin[4,5,6,7], Jing Wang[3], Han Liang[3] and Boyi Gan[1,4,5,9]

Long non-coding RNAs (lncRNAs) have emerged as critical regulators in various cellular processes. However, the potential involvement of lncRNAs in kinase signalling remains largely unknown. AMP-activated protein kinase (AMPK) acts as a critical sensor of cellular energy status. Here we show that the lncRNA *NBR2* (neighbour of *BRCA1* gene 2) is induced by the LKB1–AMPK pathway under energy stress. On energy stress, *NBR2* in turn interacts with AMPK and promotes AMPK kinase activity, thus forming a feed-forward loop to potentiate AMPK activation during energy stress. Depletion of *NBR2* attenuates energy-stress-induced AMPK activation, resulting in unchecked cell cycling, altered apoptosis/autophagy response, and increased tumour development *in vivo*. *NBR2* is downregulated and its low expression correlates with poor clinical outcomes in some human cancers. Together, the results of our study uncover a mechanism coupling lncRNAs with metabolic stress response, and provides a broad framework to understand further the regulation of kinase signalling by lncRNAs.

Mammalian genomes encode more than 10,000 long non-coding RNAs (lncRNAs), RNA molecules that are longer than 200 nucleotides and do not seem to encode proteins[1,2]. Although lncRNAs were traditionally viewed as the products that are generated from the background noise of transcription and thus exert little fitness advantage to the cells, it has become increasingly clear that these lncRNAs play important biological functions, and their dysregulation has been connected to various human diseases, including cancer[3–6].

Most current studies focus on lncRNA function in the nucleus, partly because most of the best-understood lncRNAs, such as *XIST* (ref. 7), *HOTAIR* (ref. 8), *HOTTIP* (ref. 9), are all chromatin-associated lncRNAs, which are mainly localized in the nucleus. These studies have illustrated a diverse range of functions of lncRNAs in the regulation of chromatin status, transcription and RNA processing, among others[1,10]. Many lncRNAs have also been identified in the cytosol[11]. In fact, it has been suggested that most lncRNAs probably spend most of their lifetime in the cytoplasm[1]. However, the exact functions of cytoplasmic localized lncRNAs, particularly their potential functions in the regulation of kinase signalling in the cytoplasm, remain poorly understood. In addition, although lncRNAs have been shown to regulate diverse biological processes, the role of lncRNAs in mediating a metabolic checkpoint remains largely unexplored.

The AMP-activated protein kinase (AMPK) serves as a critical sensor of cellular energy status and is activated under energy stress conditions with an increased cellular AMP/ATP ratio[12]. AMP binding to AMPK and subsequent AMPK phosphorylation at Thr172 by the upstream kinase LKB1 leads to AMPK activation[13–15]. Activated AMPK then phosphorylates a number of downstream targets to inactivate ATP-consuming anabolic processes and to activate ATP-generating catabolic processes[16]. Thus, AMPK mainly functions as a metabolic checkpoint to restore energy balance in response to energy stress. One major anabolic process inhibited by AMPK in response to energy stress is mammalian target of rapamycin complex 1 (mTORC1)-mediated protein synthesis and cell growth[17]. In response to energy stress, AMPK inactivates mTORC1 and represses protein synthesis through AMPK phosphorylation of Raptor, a component of mTORC1, and the TSC1–TSC2 complex, a negative regulator of mTORC1 (refs 18,19). AMPK also functions to promote autophagy and cell survival under energy stress through its phosphorylation of autophagy regulators, such as ULK1 (refs 20,21). As anabolic

[1]Department of Experimental Radiation Oncology, The University of Texas MD Anderson Cancer Center, 1515 Holcombe Boulevard, Houston, Texas 77030, USA. [2]Department of Biochemistry and Molecular Biology, The University of Texas Health Science Center at Houston McGovern Medical School, Houston, Texas 77030, USA. [3]Department of Bioinformatics and Computational Biology, The University of Texas MD Anderson Cancer Center, 1515 Holcombe Boulevard, Houston, Texas 77030, USA. [4]Department of Molecular and Cellular Oncology, The University of Texas MD Anderson Cancer Center, 1515 Holcombe Boulevard, Houston, Texas 77030, USA. [5]Program of Genes and Development, and Program of Cancer Biology, The University of Texas Graduate School of Biomedical Sciences, 1515 Holcombe Boulevard, Houston, Texas 77030, USA. [6]Department of Cancer Biology, Wake Forest School of Medicine, Winston-Salem, North Carolina 27157, USA. [7]Graduate Institute of Basic Medical Science, China Medical University, Taichung 404, Taiwan. [8]These authors contributed equally to this work.
[9]Correspondence should be addressed to B.G. (e-mail: bgan@mdanderson.org)

Received 24 February 2015; accepted 10 February 2016; published online 21 March 2016; DOI: 10.1038/ncb3328

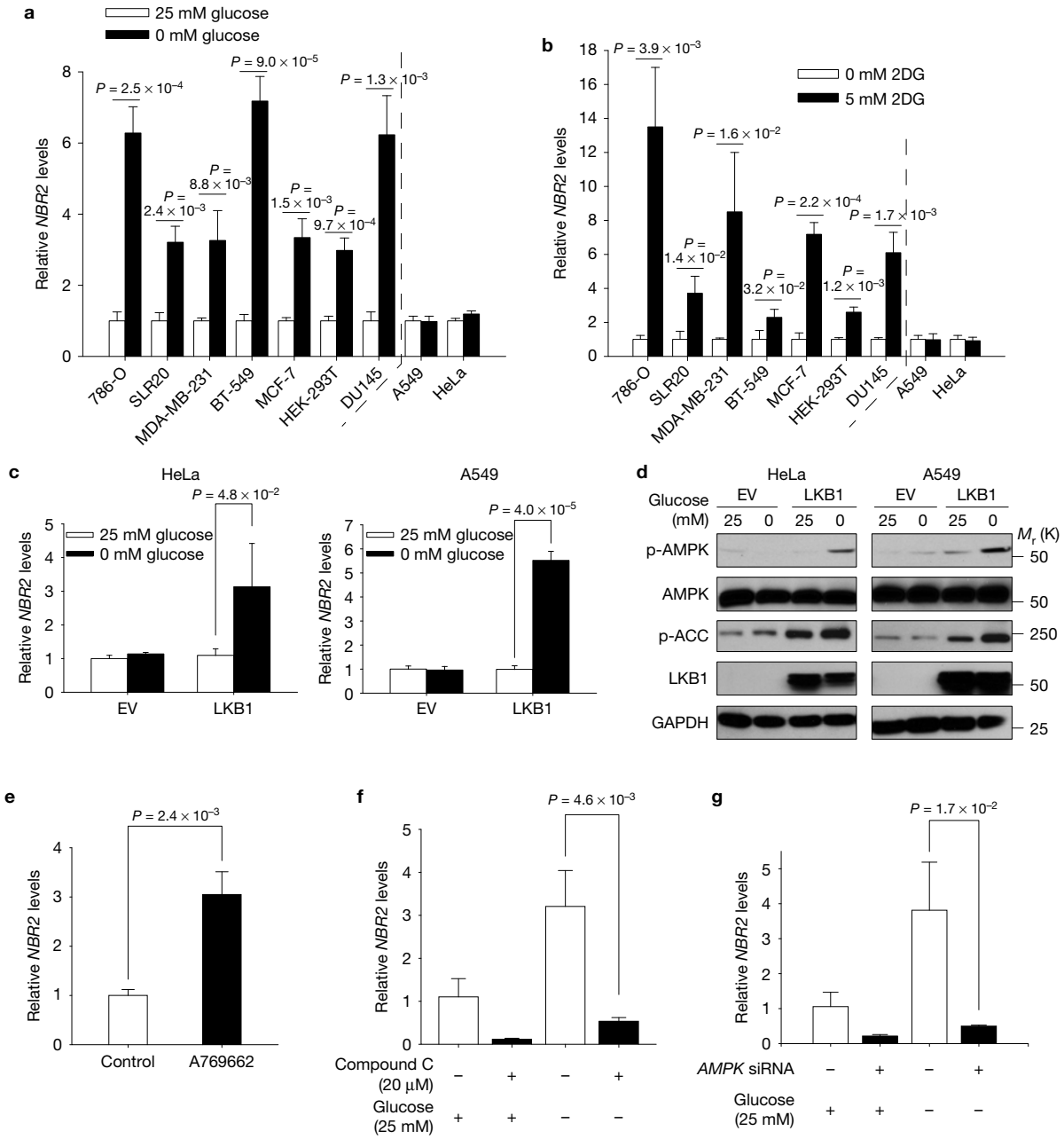

Figure 1 Energy stress induces *NBR2* expression through the LKB1–AMPK pathway. (**a**,**b**) Various cell lines were cultured in 0 or 25 mM glucose-containing medium (**a**), or 0 or 5 mM 2DG-containing medium (**b**) for 12–24 h, and then subjected to real-time PCR analysis to measure *NBR2* expression (mean ± s.d., $n = 3$ biologically independent extracts, two-tailed paired Student's *t*-test). (**c**,**d**) HeLa or A549 cells stably expressing empty vector (EV) or *LKB1* expression vectors were cultured in 25 or 0 mM glucose-containing medium, and then subjected to real-time PCR (**c**) (mean ± s.d., $n = 3$ biologically independent extracts, two-tailed paired Student's *t*-test) and western blotting analyses (**d**). (**e**) MDA-MB-231 cells treated with 100 μM A769662 were subjected to real-time PCR analysis to measure *NBR2* expression (mean ± s.d., $n = 3$ biologically independent extracts, two-tailed paired Student's *t*-test). (**f**) MDA-MB-231 cells were treated with 20 μM compound C in 25 or 0 mM glucose-containing medium for 24 h, and then subjected to real-time PCR analysis to measure *NBR2* expression (mean ± s.d., $n = 3$ biologically independent extracts, two-tailed paired Student's *t*-test). (**g**) MDA-MB-231 cells transfected with *AMPKα* or control (Ctrl) siRNA were cultured in 25 or 0 mM glucose-containing medium for 24 h, and then subjected to real-time PCR analysis to measure *NBR2* expression (mean ± s.d., $n = 3$ biologically independent extracts, two-tailed paired Student's *t*-test). Source data for **a**–**c**,**e**–**g** can be found in Supplementary Table 1. Unprocessed original scans of blots are shown in Supplementary Fig. 8.

processes, such as protein and lipid synthesis, often exert pro-growth effects in tumour development, it is well documented that AMPK activation serves to inhibit tumour development in many cancers[22]. Consistent with this, both the upstream kinase *LKB1* and downstream effectors of AMPK, such as *TSC1* and *TSC2*, are bona fide tumour suppressors and are mutated in hamartoma tumour syndromes and various sporadic cancers[23–25]. Although the biological functions of AMPK and its downstream effectors

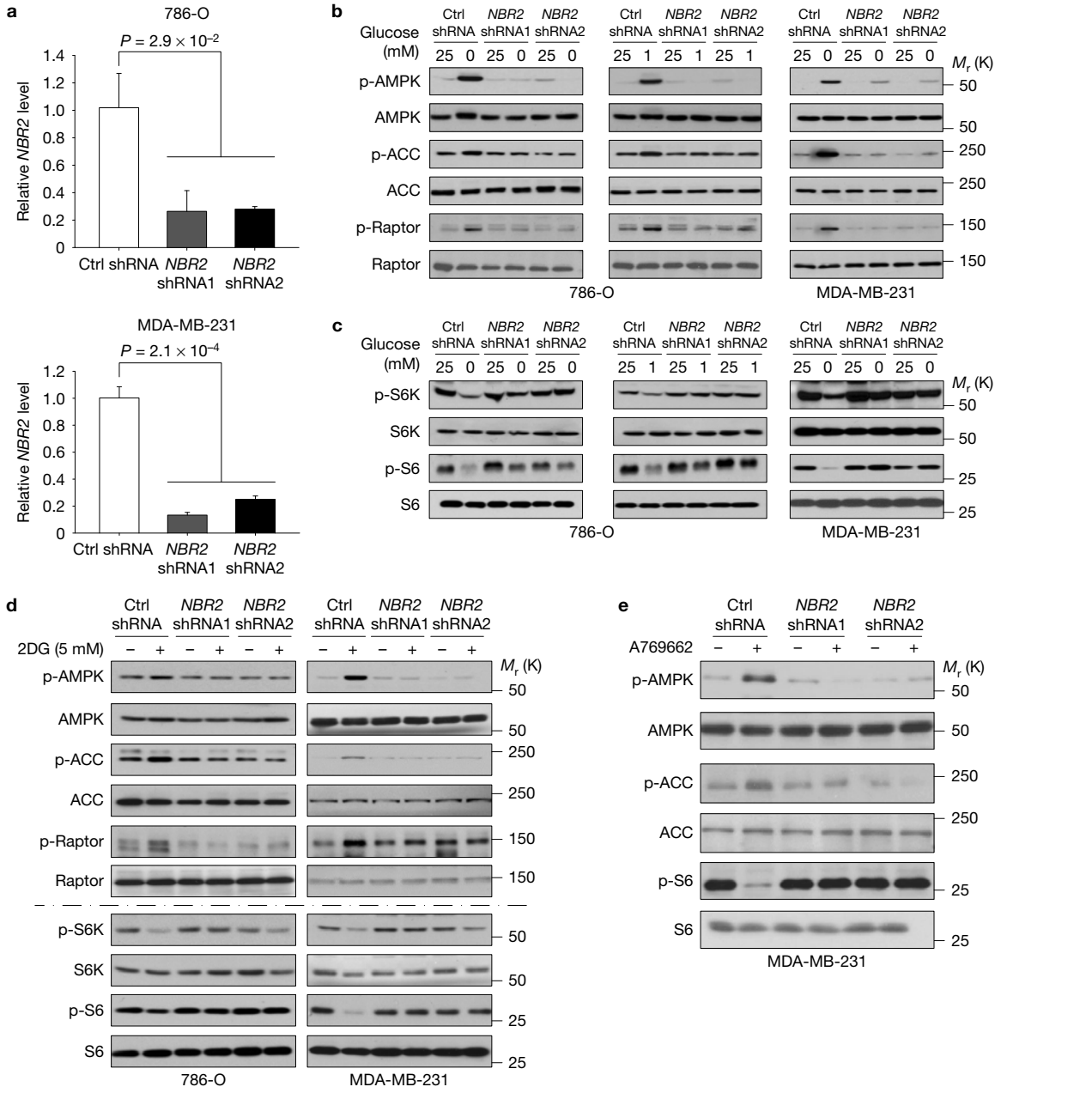

Figure 2 *NBR2* regulates AMPK–mTORC1 signalling under energy stress. (**a**) Bar graph showing *NBR2*-shRNA-mediated knockdown efficiency by real-time PCR analysis in 786-O and MDA-MB-231 cells (mean ± s.d., $n=3$ biologically independent extracts, two-tailed paired Student's *t*-test). (**b**,**c**) 786-O or MDA-MB-231 cells infected with either control shRNA or *NBR2* shRNA were cultured in medium with different concentrations of glucose for 24 h. Cell lysates were then analysed by western blotting. (**d**) 786-O or MDA-MB-231 cells infected with either control shRNA or *NBR2* shRNA were cultured in 0 or 5 mM 2DG-containing medium for 12 (for MDA-MB-231 cells) or 16 (for 786-O cells) h. Cell lysates were then analysed by western blotting. (**e**) MDA-MB-231 cells infected with either control shRNA or *NBR2* shRNA were cultured in 0 or 100 μM A769662-containing medium for 12 h. Cell lysates were then analysed by western blotting. Source data for **a** can be found in Supplementary Table 1. Unprocessed original scans of blots are shown in Supplementary Fig. 8.

involved in cancer development have been extensively studied[22,26], the regulatory mechanisms of AMPK activation by energy stress remain incompletely understood. In particular, it remains completely unknown whether any lncRNA is involved in the AMPK-mediated metabolic checkpoint.

In this study, we identify neighbour of BRCA1 gene 2 (*NBR2*) as an energy-stress-induced lncRNA and show that *NBR2* interacts with AMPK and potentiates AMPK activation under energy stress. Consistent with the tumour suppression function of AMPK, *NBR2* deficiency promotes unchecked cell cycling under energy stress and enhances tumour development *in vivo*, and *NBR2* is downregulated in human cancers. Our study thus reveals a previously unappreciated regulatory mechanism by lncRNAs to regulate kinase function and to mediate cellular energy responses.

RESULTS

Energy stress induces *NBR2* expression through the LKB1–AMPK pathway

To identify energy-stress-induced lncRNAs, we conducted an RNA sequencing experiment in 786-O cells that had been cultured in glucose-containing or glucose-free medium. Subsequent computational analysis identified *NBR2* as one of the long intergenic non-coding RNAs (lincRNAs) induced by glucose starvation. The *NBR2* gene encodes different splicing isoforms ranging from 1 to 2 kilobases (Supplementary Fig. 1). It has been shown that *NBR2* is expressed in most of the tissues examined[27]. However, the *NBR2* gene does not seem to encode a protein, and its potential function remains unknown.

Real-time PCR revealed that glucose starvation induced *NBR2* expression in different cancer cell lines, except HeLa and A549 cells, which are *LKB1* deficient (Fig. 1a). Treatment with the glucose analogue 2-deoxy-glucose (2DG), another energy stress inducer that inhibits hexokinase and blocks glycolysis, yielded similar results (Fig. 1b). Importantly, re-expression of *LKB1* in these *LKB1*-deficient cells restored energy-stress-induced *NBR2* expression (Fig. 1c,d). In addition, treatment with A769662 (an AMPK activator) induced *NBR2* expression (Fig. 1e), whereas AMPK inactivation by compound C (an AMPK inhibitor) treatment or siRNA-mediated *AMPKα* knockdown significantly attenuated glucose starvation-induced *NBR2* expression (Fig. 1f,g and Supplementary Fig. 2). Together, our results revealed that energy stress induces *NBR2* expression at least partly through the LKB1–AMPK pathway.

NBR2 regulates AMPK–mTORC1 signalling under energy stress

To study the potential function of *NBR2* in mediating energy stress response, we generated 786-O cells (a kidney cancer cell line) and MDA-MB-231 cells (a breast cancer cell line) with stable knockdown of *NBR2* (Fig. 2a). We then analysed whether knockdown of *NBR2* affected any biochemical signalling surrogate induced by energy stress, including AMPK activation. As shown in Fig. 2b, glucose starvation potently induced phosphorylation of AMPK, or the AMPK substrates acetyl-CoA carboxylase (ACC) and Raptor[18,28]. Notably, *NBR2* knockdown significantly attenuated glucose-starvation-induced phosphorylation of AMPK, ACC and Raptor. Accordingly, S6 and S6K dephosphorylation induced by glucose deprivation was significantly compromised in *NBR2* knockdown cells compared with control short hairpin RNA (shRNA)-infected cells (Fig. 2c). Finally, *NBR2* knockdown also attenuated 2DG- or A769662-treatment-induced AMPK activation and mTORC1 inactivation (Fig. 2d,e). Our results thus revealed that *NBR2* depletion attenuates energy stress-induced AMPK activation and mTORC1 inactivation, and suggested a feed-forward mechanism on *NBR2*–AMPK regulation, in which AMPK initially promotes *NBR2* expression in response to energy stress and *NBR2* in turn regulates AMPK activation under energy stress (see Discussion).

NBR2 regulates cell proliferation, apoptosis and autophagy in response to energy stress

AMPK functions as a critical metabolic checkpoint; defective AMPK signalling leads to increased cell proliferation yet decreased autophagy under conditions of energy stress, leading to apoptosis[12,20]. The aforementioned data prompted us to examine the impact of *NBR2* deficiency on cell proliferation, apoptosis and autophagy in response to energy stress. Glucose starvation markedly decreased S phase entry as measured by BrdU incorporation, and knockdown of *NBR2* significantly attenuated the reduction of S phase entry on glucose starvation (Fig. 3a–c). Thus, similar to cells with defective AMPK signalling[18], *NBR2*-deficient cells continue cycling under energy stress.

Although *NBR2* depletion did not affect apoptosis under normal culture conditions, *NBR2* deficiency induced more apoptosis under glucose starvation, as evidenced by both Annexin V staining (Fig. 3d,e) and cleaved caspase-3 western blotting (Fig. 3f). In response to energy stress, AMPK activates autophagy, a cellular adaptive response to promote cell survival under stress conditions[20,21]. Accordingly, glucose-starvation-induced GFP–LC3 puncta formation, p62 degradation and ULK1 phosphorylation were significantly compromised in *NBR2*-deficient cells (Fig. 3g,h and Supplementary Fig. 3a,b), suggesting that energy-stress-induced autophagy was defective in *NBR2*-deficient cells. Despite enhanced apoptosis, the number in *NBR2*-deficient cells increased under glucose-deprived conditions because of the increase in cycling in *NBR2*-deficient cells (Fig. 3i,j and Supplementary Fig. 3c,d). Collectively, our results showed that *NBR2* deficiency leads to enhanced cell cycling yet decreased autophagy and increased apoptosis under energy stress, which is in line with the phenotypes from cells with defective AMPK signalling, including *AMPK*-, *LKB1*-, *TSC1*- and *TSC2*-deficient cells or cells reconstituted with a Raptor mutant that is non-phosphorylatable by AMPK (refs 15,18,19,29,30).

NBR2 inhibits tumour development and is downregulated in human cancers

Given the important functions of AMPK in the regulation of human cancers[22], we next examined the potential roles of *NBR2* in tumour development. *NBR2* deficiency led to increased anchorage-independent growth, one of the hallmarks of cell transformation, with a more prominent effect under glucose-starvation conditions (Fig. 4a,b). *In vivo* experiments using the xenograft model showed that *NBR2* deficiency increased tumour development (Fig. 4c). Further analyses of the tumour samples by western blotting confirmed downregulation of AMPK and upregulation of mTORC1 signalling in *NBR2*-deficient tumours (Fig. 4d).

Consistent with the experimental results from breast and renal cancer cell lines, a survey of the RNA-seq data across different cancer types from the TCGA (The Cancer Genome Atlas) data sets revealed downregulation of *NBR2* expression in breast (BRCA) and renal (KIRC) cancer samples compared with paired normal tissue samples (Fig. 4e,f). Kaplan–Meier analysis showed that breast cancer patients with *NBR2*-low tumours had significantly worse overall survival than those with *NBR2*-high tumours (Fig. 4g). Together, our data showed that *NBR2* deficiency promotes tumour development, and *NBR2* is downregulated in human breast and renal cancers, suggesting that *NBR2* may function as a tumour suppressor in these cancers.

Energy stress induces *NBR2* interaction with AMPK

The aforementioned biological data prompted us to further study how *NBR2* regulates AMPK function. Real-time PCR analyses of

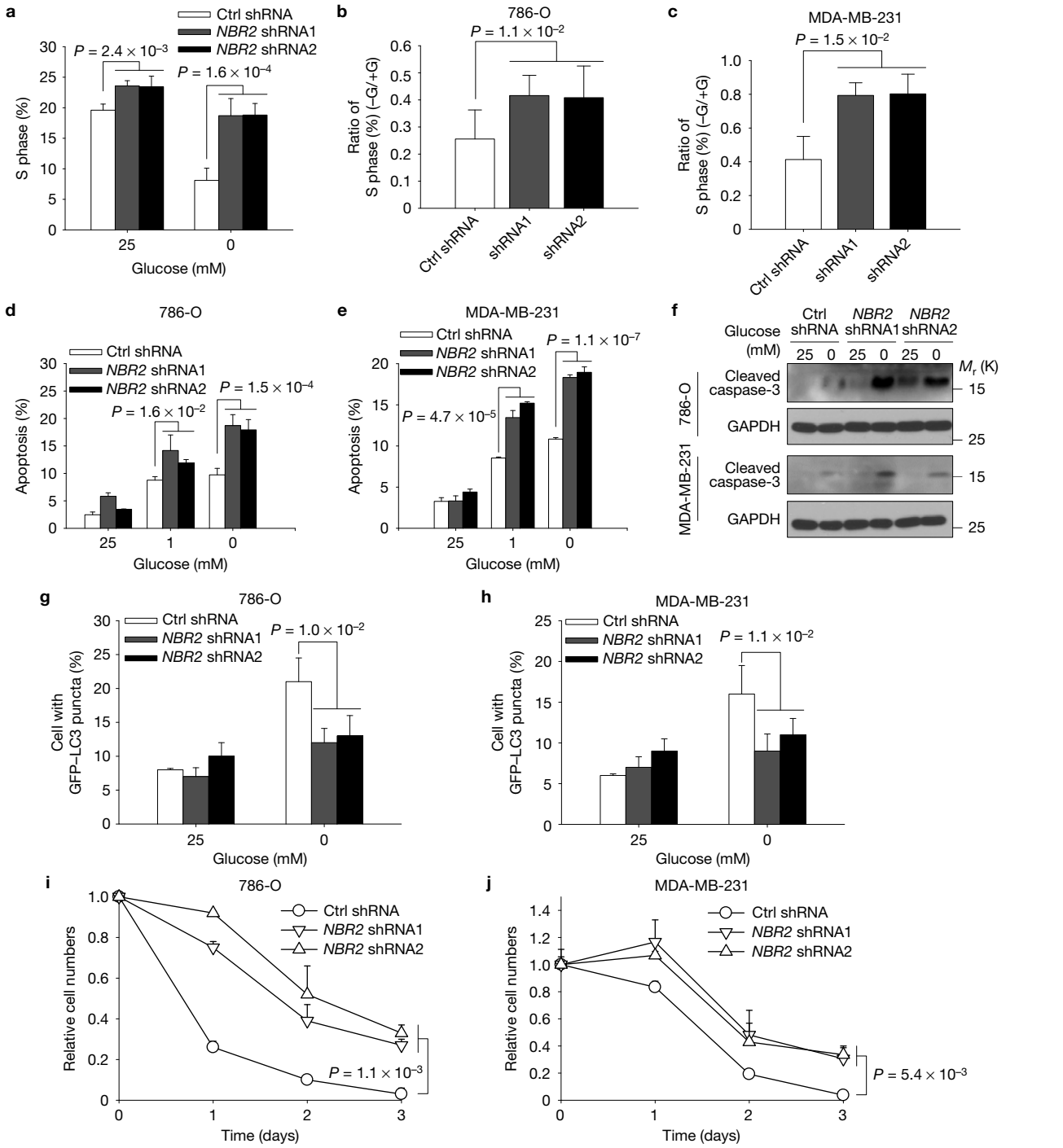

Figure 3 *NBR2* regulates cell proliferation, apoptosis and autophagy in response to energy stress. (**a**) Bar graph showing the percentages of S phase (BrdU positive) cells in control-shRNA- or *NBR2*-shRNA-infected MDA-MB-231 cells that were cultured in 25 or 0 mM glucose-containing medium for 24 h (mean ± s.d., $n=3$ biologically independent extracts, two-tailed paired Student's *t*-test). (**b**,**c**) Bar graph showing the −glucose/+glucose ratio of S phase percentages in control-shRNA- or *NBR2*-shRNA-infected 786-O cells (**b**) or MDA-MB-231 cells (**c**) (mean ± s.d., $n=3$ biologically independent extracts, two-tailed paired Student's *t*-test). (**d**–**f**) Control-shRNA- or *NBR2*-shRNA-infected 786-O cells or MDA-MB-231 cells were cultured in medium with different concentrations of glucose for 24 h, and then subjected to Annexin V/PI staining followed by FACS analysis to measure the percentages of Annexin V-positive/PI-negative cells (**d** for 786-O cells, **e** for MDA-MB-231 cells; mean ± s.d., $n=3$ biologically independent extracts, two-tailed paired Student's *t*-test), or to western blotting analysis to measure caspase-3 cleavage (**f**). (**g**,**h**) Bar graph showing the percentages of cells with LC3–GFP punctate localization in control-shRNA- or *NBR2*-shRNA-infected 786-O cells (**g**) or MDA-MB-231 cells (**h**), which were transfected with GFP–LC3 and then cultured in 25 or 0 mM glucose-containing medium for 12 (for MDA-MB-231 cells) or 18 (for 786-O cells) h (mean ± s.d., $n=5$ fields per group, each field was assessed from an independent experiment, two-tailed paired Student's *t*-test). (**i**,**j**) 786-O (**i**) or MDA-MB-231 (**j**) cells infected with either control shRNA or *NBR2* shRNA were cultured in glucose-free medium for different days as indicated, and then subjected to cell proliferation analysis (mean ± s.d., $n=3$ biologically independent extracts, two-tailed paired Student's *t*-test). Source data for **a**–**e**,**i**,**j** can be found in Supplementary Table 1. Unprocessed original scans of blots are shown in Supplementary Fig. 8.

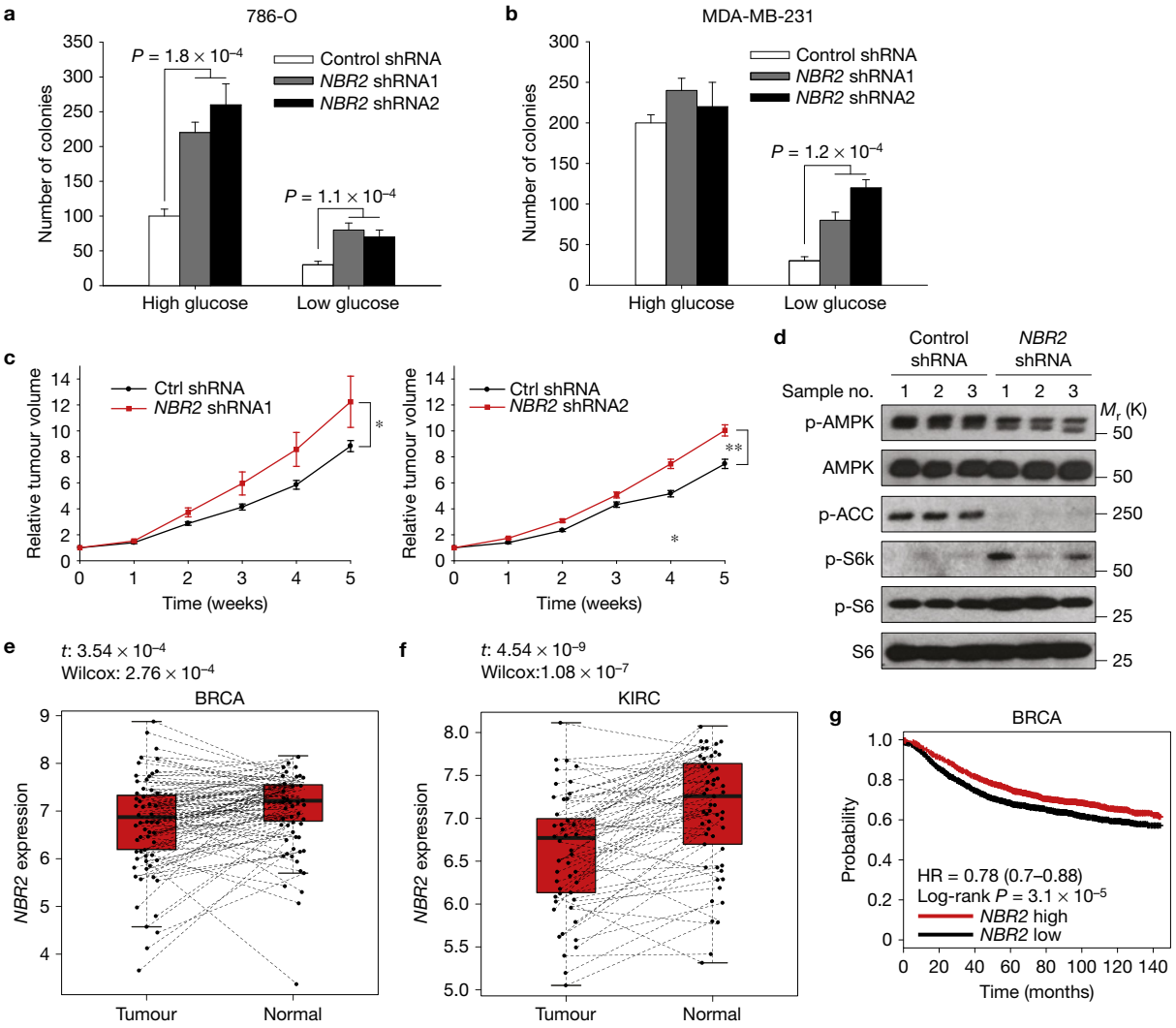

Figure 4 *NBR2* inhibits tumour development. (**a**,**b**) 786-O (**a**) or MDA-MB-231 cells (**b**) infected with either control shRNA or *NBR2* shRNA were seeded in soft agar containing high or low concentrations of glucose as indicated. Bar graph showing the mean colony numbers from the soft agar assay (mean ± s.d., $n=5$ fields per group, each field was assessed from an independent experiment, two-tailed paired Student's *t*-test). (**c**) Relative tumour volumes of MDA-MB-231 xenograft tumours infected with either control shRNA or *NBR2* shRNA at different weeks (mean ± s.e.m., $n=5$ xenograft tumours, *: $P<0.05$; **: $P<0.01$ two-tailed paired Student's *t*-test). (**d**) Protein lysates obtained from xenograft tumours infected with either control shRNA or *NBR2* shRNA at the end point were subjected to western blotting analysis as indicated. (**e**,**f**) The box plot showing the expression pattern of *NBR2* for each pair of tumour and normal samples in BRCA (**e**, $n=104$ matched pairs, Student's *t*-test and Wilcoxon test) and KIRC (**f**, $n=65$ matched pairs, Student's *t*-test and Wilcoxon test). The boxes show the median ±1 quartile, with whiskers extending to the most extreme data point within a 1.5 interquartile range from the box boundaries. (**g**) Kaplan–Meier plots of breast cancer patients stratified by the expression levels of *NBR2* ($n_{high}=1{,}767$, $n_{low}=1{,}787$, log-rank test). Unprocessed original scans of blots are shown in Supplementary Fig. 8.

fractionated nuclear and cytoplasmic RNA revealed that *NBR2* localized in both the nucleus and the cytoplasm (Fig. 5a). As expected, AMPKα showed predominant localization in the cytoplasm (Fig. 5b). AMPK exists as a heterotrimeric complex that consists of a catalytic α subunit and two regulatory β and γ subunits[31]. We thus examined whether *NBR2* can interact with any of the subunits of AMPK by RNA-pulldown assay using *in vitro*-synthesized biotinylated *NBR2*. Such analysis revealed that *NBR2* interacted with overexpressed AMPKα under glucose-starvation conditions, with minimal binding with overexpressed β or γ subunit (Fig. 5c). The RNA-pulldown assay also revealed that glucose starvation significantly increased the interaction of *NBR2* with endogenous AMPKα (Fig. 5d). As AMPKα, β and γ subunits form a very stable complex at the endogenous level, we also observed a glucose-starvation-induced binding between *NBR2* and endogenous AMPKβ and γ subunits (Fig. 5d), probably mediated by *NBR2* interaction with the endogenous AMPKα subunit. *In vitro* binding assay using purified AMPKα and *in vitro*-synthesized biotinylated *NBR2* confirmed the direct binding between *NBR2* and AMPKα (Fig. 5e). There exist at least three splicing isoforms of the *NBR2* gene (named as *NBR2* no. 1, no. 2 and no. 3; see Supplementary Fig. 1). In the RNA-pulldown experiments described above, we used the *NBR2* no. 1 splicing isoform. The RNA-pulldown experiments showed that the *NBR2* no. 2 and no. 3 splicing isoforms also interacted with AMPKα on glucose starvation (Fig. 5f). Finally,

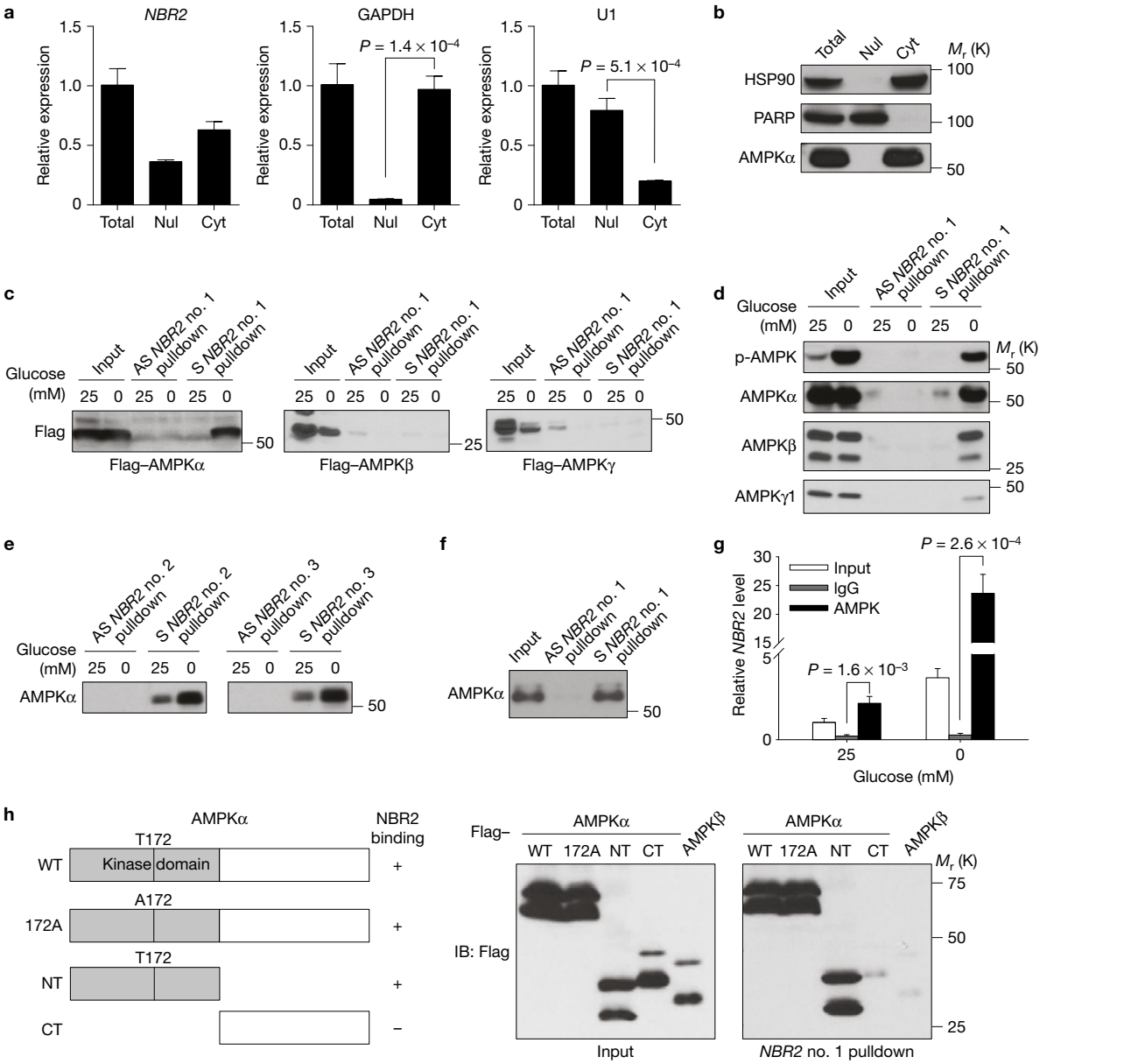

Figure 5 Energy stress induces *NBR2* interaction with AMPK. (**a**,**b**) Nuclear and cytoplasmic fractions of 786-O cells were subjected to either real-time PCR (**a**, mean ± s.d., $n = 3$ biologically independent extracts, two-tailed paired Student's *t*-test) or western blotting analysis (**b**). (**c**) *In vitro*-synthesized biotinylated sense (S) or antisense (AS) *NBR2* no. 1 was incubated with protein lysates from HEK293T cells transfected with various vectors as indicated. Precipitation reactions were conducted using streptavidin beads and then subjected to western blotting. (**d**,**e**) *In vitro*-synthesized biotinylated sense (S) *NBR2* or antisense (AS) *NBR2* with different splicing isoforms was incubated with protein lysates from 786-O cells that had been cultured in 25 or 0 mM glucose-containing medium for 24 h. Precipitation reactions were conducted using streptavidin beads and then subjected to western blotting. (**f**) *In vitro*-synthesized biotinylated sense (S) or antisense (AS) *NBR2* no. 1 was incubated with purified human AMPKα protein. Precipitation reactions were conducted using streptavidin beads and then subjected to western blotting. (**g**) 786-O cells were cultured in 0 or 25 mM glucose-containing medium for 24 h. Protein lysates were prepared and immunoprecipitated with AMPKα antibody or IgG. The RNA levels of *NBR2* in immunoprecipitates or cell lysates (input) were measured by real-time PCR (mean ± s.d., $n = 3$ biologically independent extracts, two-tailed paired Student's *t*-test). (**h**) *In vitro*-synthesized biotinylated *NBR2* no. 1 was incubated with protein lysates from HEK293T cells transfected with various vectors and subjected to glucose starvation. Precipitation reactions were conducted using streptavidin beads and then subjected to western blotting. Source data for **a**,**g** can be found in Supplementary Table 1. Unprocessed original scans of blots are shown in Supplementary Fig. 8.

RNA immunoprecipitation assay (using primers that can detect all three *NBR2* splicing isoforms) revealed an enrichment of *NBR2* in the precipitates of AMPKα compared with the IgG control, and glucose starvation substantially increased the enrichment of *NBR2* in AMPKα precipitates (note that glucose starvation resulted in a much higher fold increase of the *NBR2* level in AMPKα precipitates compared with the *NBR2* input level) (Fig. 5g).

In the experiment to map the region(s) of AMPKα that mediates AMPK interaction with *NBR2*, we showed that the kinase-domain-containing amino-terminal region, but not the carboxy-terminal

region of AMPKα, interacted with *NBR2* (Fig. 5h). Mutation of Thr172 to alanine in AMPKα did not affect AMPKα interaction with *NBR2* (Fig. 5h), indicating that AMPK phosphorylation at Thr172 is not required for AMPK–*NBR2* interaction. Together, our data revealed that glucose starvation not only induces *NBR2* expression, but also enhances *NBR2* interaction with AMPK, which is possibly mediated by *NBR2* interaction with the kinase domain of AMPKα.

NBR2 promotes AMPK kinase activity

Next we studied the underlying mechanisms by which *NBR2* regulates AMPK function. To this end, we first examined whether overexpression of *NBR2* exerts any biological effect in cells. Our experiments revealed that overexpression of any of the three *NBR2* splicing isoforms resulted in AMPK activation, mTORC1 inactivation (Fig. 6a,b), and decreased cell proliferation without affecting apoptosis under normal culture conditions (Fig. 6c). All three splicing isoforms of *NBR2* share the same first two exons located at the 5′ end of *NBR2* with distinctive exons located towards the 3′ end (Supplementary Fig. 1). Our data thus indicate that the common exons in all *NBR2* splicing isoforms might be important in mediating *NBR2* interaction with AMPK. Consistent with this, our binding mapping experiments revealed that the first exon shared by all three *NBR2* splicing isoforms is both required and sufficient to mediate *NBR2* interaction with AMPKα (Fig. 6d). Furthermore, overexpression of the T1 fragment of *NBR2* no. 1, which lacks the first exon (with 159 base pairs (bp) out of 1,045 bp full-length *NBR2* no. 1) and thus is incapable of interacting with AMPK, did not affect AMPK and mTORC1 activation status or cell proliferation, whereas in the parallel experiments, overexpression of full-length *NBR2* no. 1 exerted the expected effects on AMPK signalling (Fig. 6e,f). It seems that overexpression of the first exon alone (T4 fragment of *NBR2* no. 1) was not sufficient to activate AMPK (Supplementary Fig. 4a), suggesting that other regions in *NBR2* may be also important for *NBR2* function in the regulation of AMPK. Together, our results showed that deletion of the first exon of *NBR2* abolishes its interaction with AMPK and regulation of AMPK activation, suggesting that *NBR2* regulation of AMPK activation and downstream cellular processes is probably mediated through *NBR2* interaction with AMPK.

As LKB1 functions as the main upstream kinase of AMPK in response to energy stress[13–15], we examined whether *NBR2* regulates LKB1 interaction with AMPK. Our results showed that *NBR2* overexpression or knockdown did not affect AMPK–LKB1 interaction under either basal or glucose-starvation conditions (Supplementary Fig. 4b,c). In addition, we found that overexpression of *NBR2* in *LKB1*-deficient HeLa cells could still promote AMPK activation, and co-expression of *NBR2* and LKB1 in HeLa cells led to a synergistic increase of AMPK activation (Supplementary Fig. 4d). Together, our data suggest that *NBR2* does not regulate AMPK–LKB1 interaction and it is likely that *NBR2* operates in parallel to LKB1 to regulate AMPK activation.

Our data showing that *NBR2* interacts with the kinase domain of AMPKα (Fig. 5h) prompted the hypothesis that *NBR2* may directly regulate the kinase activity of the AMPK complex. Our data showed that bacterially purified GST–ACC (amino acids 1–130) could be readily phosphorylated by the AMPK complex precipitated from cell lysates of HEK293T cells co-transfected with AMPKα/β/γ constructs (Fig. 6g). Whereas *in vitro*-synthesized *NBR2* alone did not lead to ACC phosphorylation, the addition of *NBR2* (but not the T1 fragment of *NBR2*, the AMPK non-binding mutant) to the AMPK complex significantly increased ACC phosphorylation by AMPK (Fig. 6g). The *in vitro* kinase assay using purified AMPKα/β/γ complex and SAMS peptide as the AMPK substrate further confirmed that *NBR2* promoted AMPK *in vitro* kinase activity (Fig. 6h). Together, our data suggest that *NBR2* functions to promote AMPK kinase activity possibly through its interaction with the AMPK kinase domain.

The functional effects of *NBR2* are partially mediated by AMPK

We next sought to determine the extent to which the functional effects of *NBR2* are mediated by *NBR2* regulation of AMPK activation. We first examined whether overexpression of *NBR2* still exerted its functional effects in *AMPKα* knockdown cells. Such analyses revealed that, although overexpression of *NBR2* increased ACC phosphorylation, decreased S6 phosphorylation, and suppressed cell proliferation in control (Ctrl)-siRNA-transfected cells, such effects were attenuated in *AMPKα* knockdown (AMPK siRNA) cells (Fig. 7a,b). As a complementary approach, we also examined whether restoration of constitutively active (CA) AMPK (amino acids 1–312 of AMPKα1) would rescue any of the defects observed in *NBR2*-deficient cells. Our data revealed that overexpression of AMPK CA in *NBR2* knockdown cells restored ACC or S6 phosphorylation under glucose-starvation conditions as expected (Fig. 7c), and correspondingly, significantly rescued cell proliferation, apoptosis, and anchorage-independent growth under glucose-starvation conditions in *NBR2*-deficient cells (Fig. 7d–g). Importantly, restoration of AMPK CA in the *NBR2*-deficient background significantly attenuated the enhanced xenograft tumour development caused by *NBR2* deficiency (Fig. 7h). Taken together, our data strongly suggested that the functional effects of *NBR2* are at least partially dependent on AMPK.

DISCUSSION

AMPK exists as a heterotrimeric complex comprising of a catalytic α subunit and two regulatory β and γ subunits, in which the γ subunit directly binds to AMP in response to energy stress[31]. It has been proposed that AMP activates AMPK through at least three mechanisms: AMP binding to AMPK causes allosteric activation of AMPK, and leads to conformational change of the AMPK complex that promotes Thr172 phosphorylation in the AMPKα subunit by LKB1 and inhibits Thr172 dephosphorylation by protein phosphatases[31]. Our study reveals that lincRNA *NBR2* regulation of AMPK represents another important regulatory mechanism to control AMPK activation in response to energy stress. Here we propose a feed-forward model on *NBR2*–AMPK regulation. Specifically, energy-stress-induced initial AMPK activation does not require *NBR2*. Activated AMPK then upregulates *NBR2* expression in response to energy stress. *NBR2* in turn interacts with AMPK and promotes AMPK kinase activity under energy stress, forming a feed-forward loop to potentiate AMPK activation during chronic energy stress conditions (Supplementary Fig. 5a). *NBR2* deficiency leads to AMPK inactivation during long periods of energy stress, which promotes mTORC1 activation, cell proliferation and tumour development (Supplementary Fig. 5b). As transcription regulation in general takes a

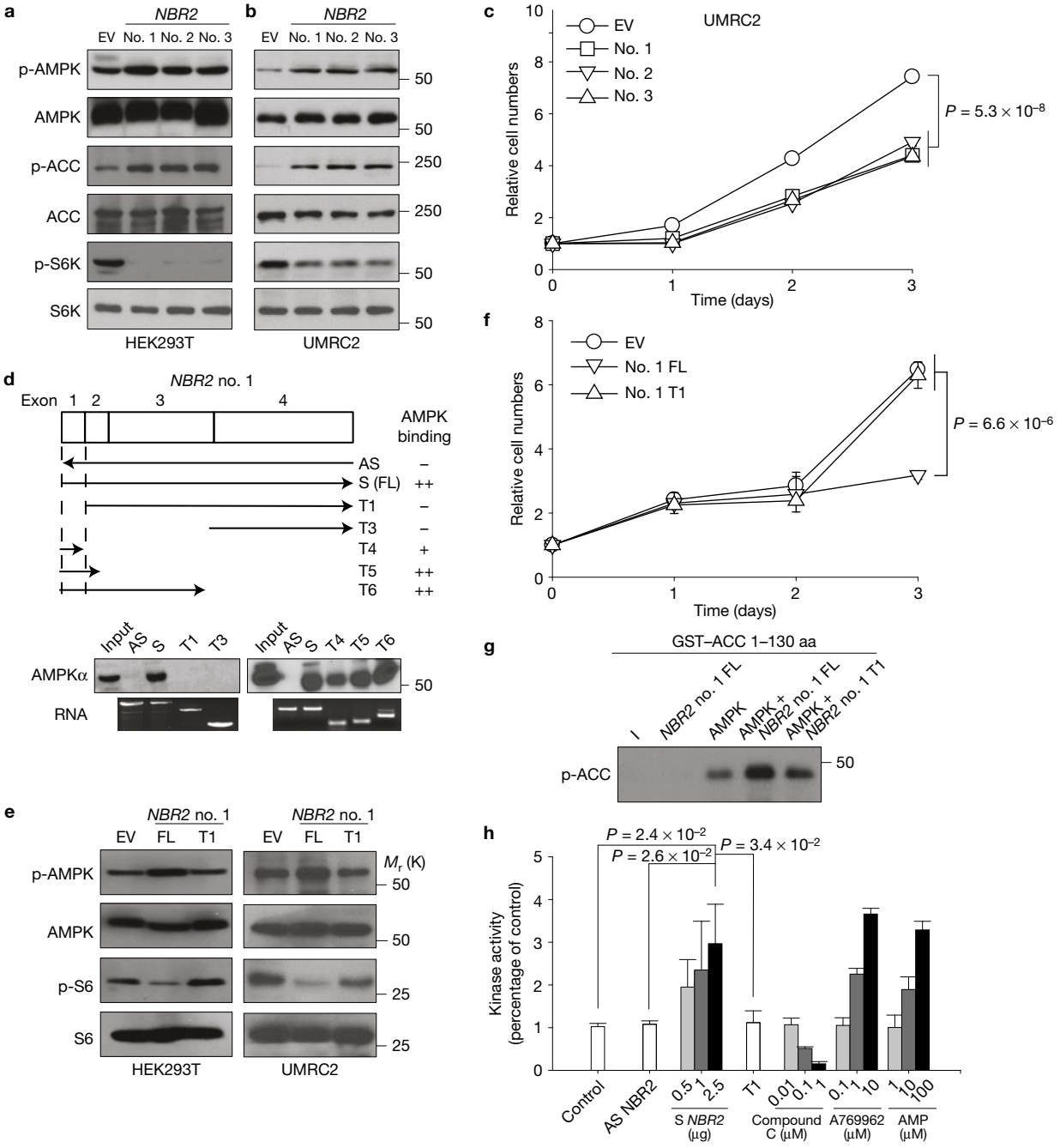

Figure 6 *NBR2* promotes AMPK kinase activity. (**a**,**b**) Protein lysates were prepared from HEK293T (**a**) or UMRC2 cells (**b**) with overexpression of EV or *NBR2* expression vectors, and analysed by western blotting. (**c**) UMRC2 cells stably expressing EV or *NBR2* expression vectors were cultured in 25 mM glucose-containing medium for different days as indicated, and then subjected to cell proliferation analysis (mean ± s.d., $n = 3$ biologically independent extracts, two-tailed paired Student's *t*-test). (**d**) Top: Schematic diagram showing different truncation mutants of *NBR2* no. 1 and the summary of their binding capabilities to AMPKα. Bottom: *In vitro*-synthesized biotinylated sense (S), antisense (AS), or different truncation (T) mutants of *NBR2* no. 1 were incubated with protein lysates from 786-O cells that had been cultured in glucose-free medium for 24 h. Precipitation reactions were conducted using streptavidin beads and then subjected to western blotting. (**e**) Protein lysates were prepared from HEK293T or UMRC2 cells with overexpression of EV, *NBR2* no. 1 full length (FL), or T1 mutant expression vectors, and analysed by western blotting. (**f**) UMRC2 cells stably expressing EV, *NBR2* no. 1 FL, or T1 mutant expression vectors were cultured in 25 mM glucose-containing medium for different numbers of days as indicated, and then subjected to cell proliferation analysis (mean ± s.d., $n = 3$ biologically independent extracts, two-tailed paired Student's *t*-test). (**g**) AMPK complex precipitated from HEK293T cells was subjected to the kinase assay in the presence of ATP, *in vitro*-synthesized RNAs and GST–ACC 1–130 amino acid fusion proteins as indicated. The kinase activity of AMPK was measured by phosphorylation of ACC at the Ser79 site. (**h**) *In vitro*-purified active human AMPK complex was subjected to *in vitro* kinase assays in the presence of ATP, SAMS peptide and *in vitro*-synthesized biotinylated sense (S)/antisense (AS)/T1 mutant (T1) *NBR2* no. 1 or several chemical compounds (compound C, A769662, AMP) as indicated (see Methods for details). The kinase activity was measured by the luminescence with a plate-reading illuminometer (mean ± s.d., $n = 3$ biologically independent extracts, two-tailed paired Student's *t*-test). Source data for **c**,**f**,**h** can be found in Supplementary Table 1. Unprocessed original scans of blots are shown in Supplementary Fig. 8.

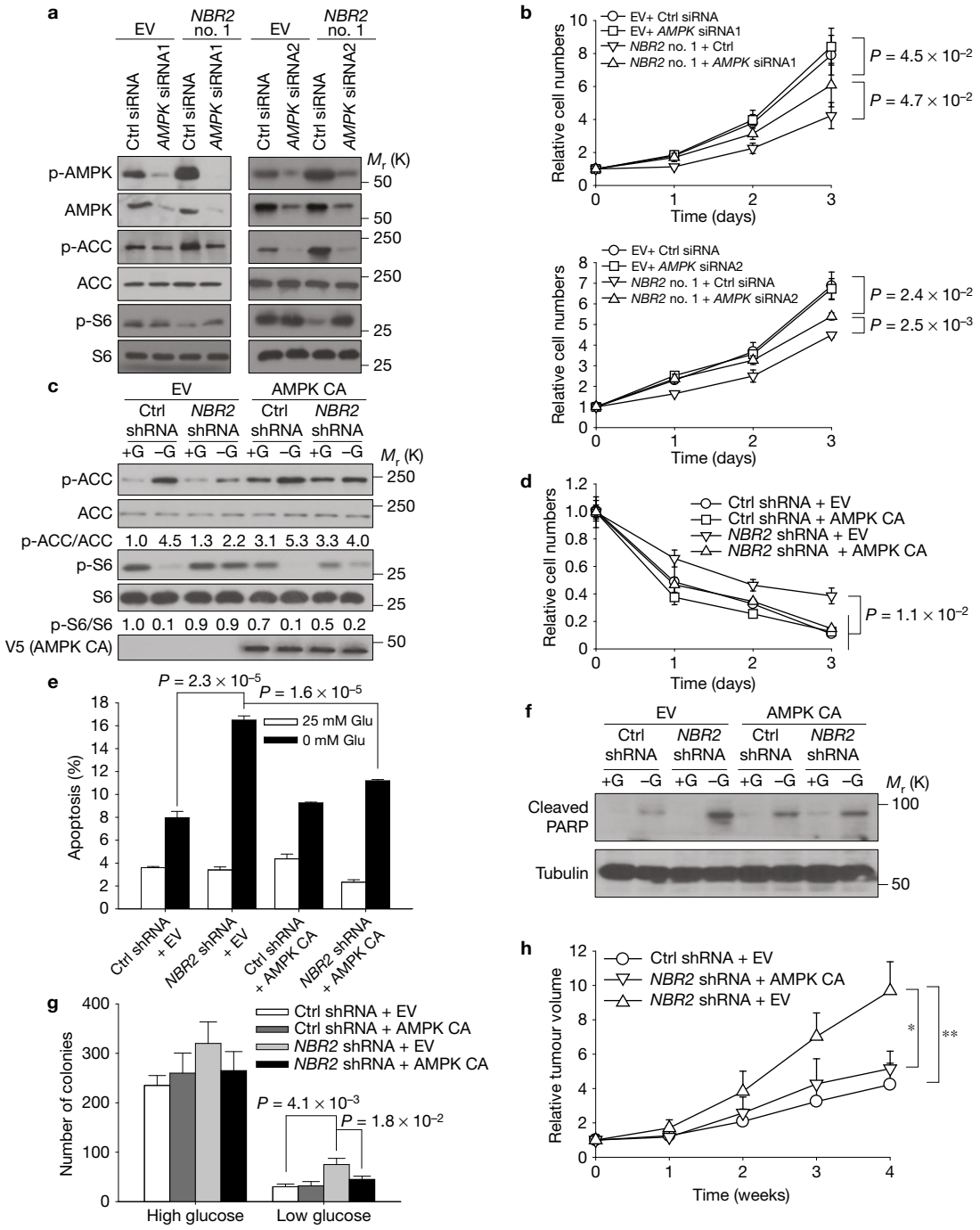

Figure 7 The functional effects of *NBR2* are partially mediated by AMPK. (**a**,**b**) UMRC2 cells stably expressing EV or *NBR2* expression vectors were transfected with *AMPK* siRNA (*AMPK* siRNA1 or siRNA2) or control (Ctrl) siRNA. Protein lysates were prepared and analysed by western blotting (**a**), or cells were cultured in 25 mM glucose-containing medium for different numbers of days as indicated, and then subjected to cell proliferation analysis (**b**) (mean ± s.d., $n=3$ biologically independent extracts, two-tailed paired Student's *t*-test). (**c**–**g**) MDA-MB-231 cells with stable expression of control (Ctrl) shRNA or *NBR2* shRNA were infected with empty vector (EV) or constitutively active AMPK (AMPK CA). These cells were cultured in 25 or 0 mM glucose-containing medium for 24 h, and protein lysates were prepared and analysed by western blotting (**c**); the cells were cultured in 0 mM glucose-containing medium for different numbers of days as indicated, and then subjected to crystal violet staining to measure cell number (**d**) (mean ± s.d., $n=3$ biologically independent extracts, two-tailed paired Student's *t*-test); the cells were cultured in 25 or 0 mM glucose-containing medium for 24 h, and then subjected to Annexin V/PI staining followed by FACS analysis to measure the percentages of Annexin V-positive/PI-negative cells (**e**) (mean ± s.d., $n=5$ fields per group, each field was assessed from an independent experiment, two-tailed paired Student's *t*-test), or to western blotting analysis to measure PARP cleavage (**f**); the cells were seeded in soft agar containing high or low concentrations of glucose as indicated. Bar graph showing the mean colony numbers from the soft agar assay (**g**) (mean ± s.d., $n=5$ fields per group, each field was assessed from an independent experiment, two-tailed paired Student's *t*-test). (**h**) Relative tumour volumes of MDA-MB-231 xenograft tumours of different genotypes at different weeks (mean ± s.d., $n=5$ xenograft tumours, *: $P<0.05$, **: $P<0.01$, two-tailed paired Student's *t*-test). Source data for **b**,**d**,**e** can be found in Supplementary Table 1. Unprocessed original scans of blots are shown in Supplementary Fig. 8.

longer time than allosteric regulation and phosphorylation events, we reason that cells may have evolved this lincRNA-involved regulatory mechanism to maintain AMPK activation during long periods of energy stress and to help cells adapt better to chronic stress conditions. In support of this model, our time course experiments revealed that *NBR2* deficiency compromised AMPK activation at later, but not earlier, time points on glucose starvation (Supplementary Fig. 6a). (Note that all of the energy stress experiments shown in our studies used 12 h or longer treatment time points.) This mirrors well with the kinetics of *NBR2* expression induction on glucose starvation (Supplementary Fig. 6b). As glucose starvation also significantly promotes *NBR2* binding to AMPK (Fig. 5), this presumably further amplifies the effect of *NBR2* to promote AMPK activation.

The *NBR2* gene was originally identified as a gene that is located near to the breast-cancer-associated gene *BRCA1*. Both genes lie head to head with each other on human chromosome 17, and the physical distance between the transcription start sites of the two genes is only 218 bp (Supplementary Fig. 1)[27]. Given the frequent mutation/deletion rates of *BRCA1* in human breast and ovarian cancers and the close proximity of the *NBR2* gene to the *BRCA1* gene, it was initially postulated that *NBR2* should be co-deleted/mutated with *BRCA1* in certain cancers (for example, see ref. 32), and *NBR2* may also play a role in tumour suppression. However, later it became clear that *NBR2* does not seem to encode a protein, and it was proposed that *NBR2* simply is a 'junk gene'[33]. Since then, its potential function in tumour biology has remained unknown. In this study, we identified *NBR2* as a lincRNA induced by energy stress, and showed that *NBR2* indeed functions to inhibit tumour development, at least in part through its regulation of AMPK activation. It is of note that *NBR2* overexpression in *AMPK*-deficient cells can still exert moderate cell proliferation suppressive effect (Fig. 7b), suggesting that *NBR2* may have other AMPK-independent function(s) to regulate cell proliferation. Identification and characterization of other *NBR2*-binding proteins or RNAs will further clarify its function.

The most popular model proposed for lncRNA function probably is the one whereby lncRNAs regulate gene expression, either in *cis* or in *trans*, through recruiting other chromatin-modification complexes or transcription factors to specific loci[34,35]. This raises the possibility that *NBR2* may regulate the transcription of the *BRCA1* gene, which resides right next to the *NBR2* gene. However, our data showed that *BRCA1* expression was not affected by either glucose starvation or *NBR2* knockdown (Supplementary Fig. 7). We should mention that, although initially it was proposed that lincRNAs mainly function to regulate neighbouring gene transcription, other studies have shown that many lincRNAs do not exert such a function[1]. Whether *NBR2* regulates any other gene transcription awaits further investigation. □

METHODS

Methods and any associated references are available in the online version of the paper.

Note: Supplementary Information is available in the online version of the paper

ACKNOWLEDGEMENTS

We thank all members of the Gan laboratory for their advice and technical assistance. This research has been supported by grants from MD Anderson Cancer Center, US Department of Defense (TS093049), Cancer Prevention & Research Institute of Texas (RP130020), National Institutes of Health (CA181196 and CA190370), Ellison Medical Foundation (AG-NS-0973-13), and Gabrielle's Angel Foundation for Cancer Research (to B.G.). B.G. is a Kimmel Scholar and an Ellison Medical Foundation New Scholar. H.Liang is supported by the National Institutes of Health (CA143883, CA175486); the R. Lee Clark Fellow Award from The Jeanne F. Shelby Scholarship Fund; a grant from the Cancer Prevention and Research Institute of Texas (RP140462); and the Mary K. Chapman Foundation and the Lorraine Dell Program in Bioinformatics for Personalization of Cancer Medicine. L.H. is supported by Cancer Prevention & Research Institute of Texas (RR150085). H.-K.L. is supported by the National Institutes of Health (CA182424 and CA193813). B.G., J.C., J.W. and H.Liang are members of the MD Anderson Cancer Center, and are supported by the National Institutes of Health Core Grant CA016672.

AUTHOR CONTRIBUTIONS

Z.-D.X. initiated the project and identified *NBR2* as an energy-stress-induced lncRNA. X.L. performed most of the experiments with assistance from Z.-D.X., H.Lee, and L.Z. J.Z. and J.W. analysed RNA-seq data set. L.H. and H.Liang conducted computational analysis on *NBR2* expression and status in human cancers. W.W., J.C., S.-W.L. and H.-K.L. provided reagents. B.G. supervised the study. X.L., Z.-D.X. and B.G. designed the experiments and wrote the manuscript. All authors commented on the manuscript.

COMPETING FINANCIAL INTERESTS

The authors declare no competing financial interests.

Published online at http://dx.doi.org/10.1038/ncb3328
Reprints and permissions information is available online at www.nature.com/reprints

1. Ulitsky, I. & Bartel, D. P. lincRNAs: genomics, evolution, and mechanisms. *Cell* **154,** 26–46 (2013).
2. EP Consortium, An integrated encyclopedia of DNA elements in the human genome. *Nature* **489,** 57–74 (2012).
3. Batista, P. J. & Chang, H. Y. Long noncoding RNAs: cellular address codes in development and disease. *Cell* **152,** 1298–1307 (2013).
4. Gupta, R. A. *et al.* Long non-coding RNA HOTAIR reprograms chromatin state to promote cancer metastasis. *Nature* **464,** 1071–1076 (2010).
5. Huarte, M. *et al.* A large intergenic noncoding RNA induced by p53 mediates global gene repression in the p53 response. *Cell* **142,** 409–419 (2010).
6. Prensner, J. R. *et al.* Transcriptome sequencing across a prostate cancer cohort identifies PCAT-1, an unannotated lincRNA implicated in disease progression. *Nat. Biotechnol.* **29,** 742–749 (2011).
7. Engreitz, J. M. *et al.* The Xist lncRNA exploits three-dimensional genome architecture to spread across the X chromosome. *Science* **341,** 1237973 (2013).
8. Rinn, J. L. *et al.* Functional demarcation of active and silent chromatin domains in human HOX loci by noncoding RNAs. *Cell* **129,** 1311–1323 (2007).
9. Wang, K. C. *et al.* A long noncoding RNA maintains active chromatin to coordinate homeotic gene expression. *Nature* **472,** 120–124 (2011).
10. Guttman, M. & Rinn, J. L. Modular regulatory principles of large non-coding RNAs. *Nature* **482,** 339–346 (2012).
11. van Heesch, S. *et al.* Extensive localization of long noncoding RNAs to the cytosol and mono- and polyribosomal complexes. *Genome Biol.* **15,** R6 (2014).
12. Hardie, D. G., Ross, F. A. & Hawley, S. A. AMPK: a nutrient and energy sensor that maintains energy homeostasis. *Nat. Rev. Mol. Cell Biol.* **13,** 251–262 (2012).
13. Hawley, S. A. *et al.* Complexes between the LKB1 tumor suppressor, STRAD α/β and MO25 α/β are upstream kinases in the AMP-activated protein kinase cascade. *J. Biol.* **2,** 28 (2003).
14. Woods, A. *et al.* LKB1 is the upstream kinase in the AMP-activated protein kinase cascade. *Curr. Biol.* **13,** 2004–2008 (2003).
15. Shaw, R. J. *et al.* The tumor suppressor LKB1 kinase directly activates AMP-activated kinase and regulates apoptosis in response to energy stress. *Proc. Natl Acad. Sci. USA* **101,** 3329–3335 (2004).
16. Hardie, D. G., Schaffer, B. E. & Brunet, A. AMPK: an energy-sensing pathway with multiple inputs and outputs. *Trends Cell Biol.* **26,** 190–201 (2015).
17. Laplante, M. & Sabatini, D. M. mTOR signaling in growth control and disease. *Cell* **149,** 274–293 (2012).
18. Gwinn, D. M. *et al.* AMPK phosphorylation of raptor mediates a metabolic checkpoint. *Mol. Cell* **30,** 214–226 (2008).
19. Inoki, K., Zhu, T. & Guan, K. L. TSC2 mediates cellular energy response to control cell growth and survival. *Cell* **115,** 577–590 (2003).
20. Egan, D. F. *et al.* Phosphorylation of ULK1 (hATG1) by AMP-activated protein kinase connects energy sensing to mitophagy. *Science* **331,** 456–461 (2011).
21. Kim, J., Kundu, M., Viollet, B. & Guan, K. L. AMPK and mTOR regulate autophagy through direct phosphorylation of Ulk1. *Nat. Cell Biol.* **13,** 132–141 (2011).
22. Shackelford, D. B. & Shaw, R. J. The LKB1-AMPK pathway: metabolism and growth control in tumour suppression. *Nat. Rev. Cancer* **9,** 563–575 (2009).

23. Huang, J. & Manning, B. D. The TSC1-TSC2 complex: a molecular switchboard controlling cell growth. *Biochem. J.* **412,** 179–190 (2008).
24. Hezel, A. F. & Bardeesy, N. LKB1; linking cell structure and tumor suppression. *Oncogene* **27,** 6908–6919 (2008).
25. Alessi, D. R., Sakamoto, K. & Bayascas, J. R. LKB1-dependent signaling pathways. *Annu. Rev. Biochem.* **75,** 137–163 (2006).
26. Faubert, B. *et al.* AMPK is a negative regulator of the Warburg effect and suppresses tumor growth *in vivo*. *Cell Metab.* **17,** 113–124 (2013).
27. Xu, C. F. *et al.* Isolation and characterisation of the NBR2 gene which lies head to head with the human BRCA1 gene. *Hum. Mol. Genet.* **6,** 1057–1062 (1997).
28. Sim, A. T. & Hardie, D. G. The low activity of acetyl-CoA carboxylase in basal and glucagon-stimulated hepatocytes is due to phosphorylation by the AMP-activated protein kinase and not cyclic AMP-dependent protein kinase. *FEBS Lett.* **233,** 294–298 (1988).
29. Bungard, D. *et al.* Signaling kinase AMPK activates stress-promoted transcription via histone H2B phosphorylation. *Science* **329,** 1201–1205 (2010).
30. Corradetti, M. N., Inoki, K., Bardeesy, N., DePinho, R. A. & Guan, K. L. Regulation of the TSC pathway by LKB1: evidence of a molecular link between tuberous sclerosis complex and Peutz-Jeghers syndrome. *Genes Dev.* **18,** 1533–1538 (2004).
31. Hardie, D. G. AMPK-sensing energy while talking to other signaling pathways. *Cell Metab.* **20,** 939–952 (2014).
32. Gad, S. *et al.* Characterisation of a 161 kb deletion extending from the NBR1 to the BRCA1 genes in a French breast-ovarian cancer family. *Hum. Mutat.* **21,** 654 (2003).
33. Jin, H. *et al.* Structural evolution of the BRCA1 genomic region in primates. *Genomics* **84,** 1071–1082 (2004).
34. Pandey, R. R. *et al.* Kcnq1ot1 antisense noncoding RNA mediates lineage-specific transcriptional silencing through chromatin-level regulation. *Mol. Cell* **32,** 232–246 (2008).
35. Feng, J. *et al.* The Evf-2 noncoding RNA is transcribed from the Dlx-5/6 ultraconserved region and functions as a Dlx-2 transcriptional coactivator. *Genes Dev.* **20,** 1470–1484 (2006).

METHODS

Cell culture studies. Human kidney cancer cell lines, human breast cancer cell lines, human prostate cancer cell lines, human embryonic kidney 293 cells used in this study were mostly obtained from American Type Culture Collection (ATCC). All of the cell lines were free of mycoplasma contamination (tested by the vendors using the MycoAlert kit from Lonza). No cell lines used in this study are found in the database of commonly misidentified cell lines (ICLAC and NCBI Biosample) based on short tandem repeat (STR) profiling performed by vendors. HeLa or A549 cells with expression of empty vector or *Lkb1* expression vectors were described in ref. 36. siRNA and plasmid transfections were performed using Lipofectamine 3000 (Life Technologies). Lentiviruses or retroviruses were produced in HEK293T cells with packing mix (ViraPower Lentiviral Expression System, Invitrogen) and used to infect target cells as per the manufacturer's instructions. For glucose-starvation experiments, cells were cultured in DMEM with different concentrations of glucose (0, 1, or 25 mM) + 10% dialysed FBS. To measure apoptosis, the cells were stained by the Annexin V kit as per the manufacturer's instructions (BD Bioscience)[37]. Briefly, treated cells were washed with PBS twice and then 1×10^6 cells were resuspended in 100 µl of 1× binding buffer. FITC-labelled Annexin V and propidium iodide were added to samples and incubated in the dark for 15 min at room temperature. Subsequently, cells were subjected to FACS analysis. Cell cycle analysis was carried out as previously reported using the FITC BRDU Flow Kit (BD Bioscience)[38,39]. Cell growth and soft agar assays were conducted as described in our previous publications[40,41]. Briefly, for cell growth assay, cells were plated in 24-well plates and growth was determined by crystal violet staining. Cells were stained with 0.1% crystal violet (Sigma) solution for 15 min at room temperature. Stained crystal violet was then extracted with 10% acetic acid and the intensity of the colour was measured by photospectrometry at OD_{595}. To assess anchorage-independent growth, 10,000 cells per well in 0.4% agarose on top of a bottom layer of 0.7% agarose were seeded in triplicate wells of 6-well plates. On the formation of colonies, soft agar plates were stained with iodonitrotetrazolium chloride (Sigma) and the colonies were counted manually.

Constructs and reagents. shRNAs targeting human *NBR2* (NM_005821.2-615s1c1, NM_005821.2-514s1c1) were purchased from Sigma (note that these two shRNAs target splicing isoforms no. 1 and no. 3 of *NBR2*, and can still achieve good knockdown efficiency when measured by real-time PCR primer set designed to detect all three splicing isoforms of *NBR2*). siRNAs targeting AMPKα were purchased from Origene (SR303721, SR303722). All three splicing isoforms of *NBR2* were obtained from Thermo Fisher Scientific (MGC human *NBR2* sequence-verified cDNAs, clone ID: 6452095, 4339497, 4826858) and then were subcloned into Lentiviral vector pLVX (Clontech). AMPKα, AMPKβ and AMPKγ entry plasmids were obtained from the Human ORFeome V5.1 library. The entry clones were subsequently recombined into gateway-compatible destination expression vectors with Flag tag through LR Gateway Technology (Invitrogen). cDNA corresponding to amino acids 1–312 of AMPKα1 was cloned into entry vector, and was subsequently recombined into gateway-compatible destination expression vectors with V5 tag through LR Gateway Technology (Invitrogen). Active human AMPKα2 protein and active human AMPKα1+AMPKβ1+AMPKγ1 protein were purchased from Abcam (ab79803, ab126916). 2-Deoxy-D-glucose and compound C were purchased from Sigma (D6134, P5499). A-769662 was purchased from LC laboratories (A-1803).

Quantitative real-time PCR and RNA immunoprecipitation (RIP) assay. Total RNA was extracted from cells using RNeasy (Qiagen) and first-strand cDNA was prepared with the High Capacity cDNA Reverse Transcription Kit (Applied Biosystems, ABI). Real-time PCR was performed using the QuantiTect SYBR Green PCR kit (Qiagen) or TaqMan Universal PCR Master Mix (ABI), and was run on the Stratagene MX3000P. For quantification of gene expression, the $2^{-\Delta\Delta Ct}$ method was used. GAPDH expression was used for normalization. RIP assay was performed with the Magna RIP RNA-Binding Protein Immunoprecipitation Kit (Millipore). Briefly, cells were lysed in RIP lysis buffer. Then the lysates were immunoprecipitated with antibody or IgG along with protein magnetic beads. After proteinase K digestion, the RNAs pulled down with proteins were purified by phenol chloroform extraction and precipitated in ethanol. The RNAs were then resuspended in RNAse-free water and cDNA was synthesized and subjected to real-time PCR to detect *NBR2* or *GAPDH* (internal control) transcripts. The RNA level was normalized with input (10%).

RNA-pulldown assays. Biotin-labelled RNAs were synthesized by the Scientific TranscriptAid T7 High Yield Transcription Kit (Thermo). PCR primers with T7 promoters were used to amplify DNA templates for RNA synthesis, RNA transcribed *in vitro* with biotin RNA labelling mix and T7 RNA polymerase, treated with RNase-free DNase I (Roche), and purified with the RNeasy Mini Kit (Qiagen). Cells lysates or purified proteins were incubated with biotin-labelled RNAs overnight. The proteins associated with biotin-labelled RNAs were then pulled down with streptavidin magnetic beads (Thermo) after 1-h incubation. The proteins was then washed and used for western blot analysis.

Western blot analysis. Tissues were lysed with RIPA buffer (20 mM Tris pH 7.5, 150 mM NaCl, 1% Nonidet P-40, 0.5% sodium deoxycholate, 1 mM EDTA, 0.1% SDS) containing complete mini protease inhibitors (Roche) and phosphatase inhibitor cocktail (Calbiochem). Cultured cells were lysed with NP40 buffer (150 mM sodium chloride, 1.0% NP-40, 50 mM Tris, pH 8.0) containing complete mini protease inhibitors (Roche) and phosphatase inhibitor cocktail (Calbiochem). Western blots were obtained using 20 to 40 µg of lysate protein. The following antibodies were used in this study: anti-FLAG tag (M2) mouse monoclonal antibody (Sigma-Aldrich, F3165, 1:5,000 dilution), monoclonal anti-vinculin antibody (Sigma-Aldrich, V4505, 1:5,000 dilution), phospho-acetyl-CoA carboxylase (Ser79) antibody (Cell Signaling Technology, 3661S, 1:1,000 dilution), acetyl-CoA carboxylase antibody (Cell Signaling Technology, 3662S, 1:1,000 dilution), phospho-p70 S6 kinase (Thr389) antibody (Cell Signaling Technology, 9205S, 1:1,000 dilution), phospho-AMPKα (Thr172) (40H9) rabbit monoclonal antibody (Cell Signaling Technology, 2535S, 1:1,000 dilution), AMPKα (D63G4) rabbit monoclonal antibody (Cell Signaling Technology, 5832S, 1:1,000 dilution), AMPKα (F6) mouse monoclonal antibody (Cell Signaling Technology, 2793S, 1:1,000 dilution), AMPKβ1/2 (57C12) rabbit monoclonal antibody (Cell Signaling Technology, 4150S, 1:1,000 dilution), AMPKγ1 antibody (Cell Signaling Technology, 4187S, 1:1,000 dilution), phospho-Raptor (Ser792) antibody (Cell Signaling Technology, 2083S, 1:1,000 dilution), Raptor (24C12) rabbit monoclonal antibody (Cell Signaling Technology, 2280S, 1:1,000 dilution), phospho-S6 ribosomal protein (Ser240/244) (D68F8), XP rabbit monoclonal antibody (Cell Signaling Technology, 5364S, 1:5,000 dilution), S6 ribosomal protein (5G10) rabbit monoclonal antibody (Cell Signaling Technology, 2217S, 1:5,000 dilution), ULK1 (D8H5) rabbit monoclonal antibody (Cell Signaling Technology, 8054 S, 1:1,000 dilution), phospho-ULK1 (Ser555) (D1H4) rabbit monoclonal antibody (Cell Signaling Technology, 5869S, 1:1,000 dilution), phospho-ULK1 (Ser757) antibody (Cell Signaling Technology, 6888S, 1:1,000 dilution), cleaved PARP (Asp214) antibody (Human Specific) (Cell Signaling Technology, 9541S, 1:2,000 dilution), PARP antibody (Cell Signaling Technology, 9542S, 1:2,000 dilution), cleaved caspase-3 (Asp175) (5A1E) rabbit monoclonal antibody (Cell Signaling Technology, 9664S, 1:500 dilution), FLCN (D14G9) rabbit monoclonal antibody (Cell Signaling Technology, 3697S, 1:2,000 dilution), HSP90 (C45G5) rabbit monoclonal antibody no. 4877(Cell Signaling Technology, 4877S, 1:1,000 dilution), GAPDH (D16H11) XP rabbit monoclonal antibody (Cell Signaling Technology, 5174S, 1:5,000 dilution), p70 S6 kinase α antibody (C-18) (Santa Cruz Biotechnology, sc-230, 1:1,000 dilution), SQSTM1 antibody (H-290) (Santa Cruz Biotechnology, sc-52275, 1:2,000 dilution), LKB1 antibody (E-9) (Santa Cruz Biotechnology, sc-374334, 1:2,000 dilution).

Subcellular fractionation. Cells were collected using trypsin and washed twice with PBS. Cell pellets were lysed in buffer I containing 20 mM HEPES, 10 mM KCl, 2 mM $MgCl_2$ and 0.5% NP40. After centrifugation, supernatants were collected as cytoplasmic lysis. Pellets were further lysed in buffer II containing 0.5 M NaCl, 20 mM HEPES, 10 mM KCl, 2 mM $MgCl_2$ and 0.5% NP40. Supernatants were collected as nuclear lysis by centrifugation. Cytoplasmic and nuclear fractions were split for RNA extraction and real-time PCR or protein extraction and western blotting. HSP90 and PARP were used as markers of cytoplasm and nucleus in western blotting. GAPDH and U1 were used as markers of cytoplasm and nucleus in real-time PCR.

Immunofluorescence. Cells were cultured on glass coverslips in 6-well plates, washed once with PBS, and fixed in 4% paraformaldehyde for 30 min. Coverslips were mounted using Immu-mount (Thermo Shandon) and images were captured using an Olympus confocal microscope. For quantification of autophagic cells, cells with >10 GFP–LC3 punctuate dots were considered positive. Positive cells was counted and expressed as a percentage of total autophagic cells.

AMPK kinase assay. *In vitro* AMPK kinase activity was assessed using the Promega AMPK (A1/B1/G1) Kinase Enzyme System (V1921) according to the manufacturer's instructions. In the kinase assay using the ACC fragment, bacterially purified GST–ACC 1–130 amino acid protein was dialysed against 20 mM Tris-HCl, pH 8.0 and 10% glycerol at 4 °C overnight. For AMPK kinase assay, SFB–AMPKα1, Flag–AMPKβ2 and Flag–AMPKγ1 plasmids were co-transfected into HEK293T cells. Cells were lysed 48 h after transfection. AMPK complex was pulled down by S protein beads and subjected to the kinase assay in the presence of 500 µM cold ATP, 10 µg *in vitro* synthesized RNAs and 1 µg GST fusion proteins mentioned above. The reaction mixture was incubated at 30 °C for 30 min, terminated with SDS-loading buffer and subjected to SDS–PAGE for western blot analysis. Phosphorylation of ACC at the Ser79 site was determined by ACC Ser79 phospho-specific antibody.

DOI: 10.1038/ncb3328

Xenograft model. All animal experiments with female athymic Nude–Foxn1^{nu} mice (6-week-old) were performed in accordance with a protocol approved by the Institutional Animal Care and Use Committee of MD Anderson Cancer Center, which is in full compliance with policies of the Institutional Animal Core and Use Committee (IACUC). Animals arriving in our facility were randomly put into cages with five mice each. They were implanted with respective tumour cells in the unit of cages, which were randomly selected. MDA-MB-231 cells were counted and suspended at 1.0×10^7 ml^{-1} in PBS, approximately one million cells were injected subcutaneously into the flank of each mouse with different genotypes, five mice per group. Tumour volume measurement was initiated at two weeks after injection (defined as starting time point: week 0). Tumour progression was then monitored by bi-dimensional tumour measurements every five days using a calliper until the endpoint. Mice were euthanized at the endpoint and the tumours were excised for further experiments. The tumour volume was calculated according to the equation $v = \text{length} * \text{width}^2 * 1/2$. The tumour volume at week n is expressed as relative tumour volume (RTV) and calculated according to the following formula: RTV = TV_n/TV_0, where TVn is the tumour volume at week n and TV0 is the tumour volume at week 0. The investigators were not blinded to allocation during experiments and outcome assessment.

RNA-seq and computational analysis. RNA-seq was performed at the Sequencing and Non-Coding RNA Program at the MD Anderson Cancer Center using Applied Biosystems SOLiD Next Generation Sequencing platform. LifeScope v2.5.1 was used to align the reads to the genome, generate raw counts corresponding to each known gene (total 23,080 genes, including 4,325 non-coding genes), and calculate the RPKM (reads per kilobase per million) values. We considered only non-coding genes that expressed at relatively high levels (RPKM > 2) and showed >2- or <0.5-fold changes between control and treatment cells. This identified a list of 17 upregulated and 39 downregulated non-coding RNAs.

Kaplan–Meier survival analysis of cancer patients. We used data sets of 4,142 breast tumours that had previously been profiled by Affymetrix microarray analysis (www.kmplot.com)[42]. *NBR2* expression (probe set ID: 207631_at) was divided by the median into high versus low expression. Survival analysis by Kaplan–Meier and Cox proportional hazard analysis were performed.

TCGA data analysis. We downloaded the level-3 gene expression data for *NBR2* from the TCGA pan-cancer project Synapse (Synapse ID: syn300013) for breast (BRCA) and kidney cancer (KIRC). We used paired Student's t-test to detect the statistical difference between matched tumour and normal samples. We used log-rank tests to detect the overall survival difference between patient groups.

Accession numbers. RNA-seq data sets (786-O cells with or without glucose treatment) have been deposited in the Gene Expression Omnibus website with accession code GSE77415. The data sets used in Fig. 4g were generated from ref. 43.

Oligonucleotide sequences, probes and primers (forward and reverse). qPCR primers for gene expression and RIP:

NBR2-Forward: 5′-GGAGGTCTCCAGTTTCGGTA-3′

NBR2-Reverse: 5′-TTGATGTGTGCTTCCTGGG-3′

(note that this real-time PCR primer set for *NBR2* is designed to detect all three splicing isoforms of *NBR2*)

GAPDH-Forward: 5′-CCATGGGGAAGGTGAAGGTC-3′

GAPDH-Reverse: 5′-GAAGGGGTCATTGATGGCAAC-3′

U1-Forward: 5′-TCCCAGGGCGAGGCTTATCCATT-3′

U1-Reverse: 5′-GAACGCAGTCCCCCACTACCACAAAT-3′

BRCA1-Forward: 5′-TGTGCTTTTCAGCTTGACACAGG-3′

BRCA1-Reverse: 5′-CGTCTTTTGAGGTTGTATCCGCTG-3′

Primers for RNA-pulldown assay:

NBR2 no. 1-Forward: 5′-TAATACGACTCACTATAGGG AGGGGTCCAGTT GCGGCTTAT-3′

NBR2 no. 1-Reverse: 5′-AGTTT ACTTA CTATT GCTGA-3′

NBR2 no. 1 Antisense-Forward: 5′-TAATACGACTCACTATAGGG AGTTTA CTTACTATT GCTGA-3′

NBR2 no. 1 Antisense-Reverse: 5′-GGGTCCAGTTGCGGCTTAT-3′

NBR2 no. 2-Forward: 5′-TAATACGACTCACTATAGGG GTTGCGGCTTAT TGCATCACA-3′

NBR2 no. 2-Reverse: 5′-ACTATTGCTGATTTATTACAAAGGA-3′

NBR2 no. 2 Antisense-Forward: 5′-TAATACGACTCACTATAGGG ACTATT GCTGATTTA TTACAAAGGA-3′

NBR2 no. 2 Antisense-Reverse: 5′-GTTGCGGCTTATTGCATCACA-3′

NBR2 no. 3-Forward: 5′-TAATACGACTCACTATAGGG AGCGGGGTTGCG GCTTATT-3′

NBR2 no. 3-Reverse: 5′-TGGGATTGAGGAGGATCTTT-3′

NBR2 no. 3 Antisense-Forward: 5′-TAATACGACTCACTATAGGG TGGGAT TGAGGAGGA TCTTT-3′

NBR2 no. 3 Antisense-Reverse: 5′-GGGTTGCGGCTTATTGCATC-3′

NBR2 no. T1-Forward: 5′-TAATACGACTCACTATAGGG GTAAAAGTTTT CATTTGATCTG AA-3′

NBR2 no. T1-Reverse: 5′-AGTTT ACTTA CTATT GCTGA-3′

NBR2 no. T3-Forward: 5′-TAATACGACTCACTATAGGG TTTGCTGAGGA TAATGGCCT-3′

NBR2 no. T3-Reverse: 5′-AGTTT ACTTA CTATT GCTGA-3′

NBR2 no. T4-Forward: 5′-TAATACGACTCACTATAGGG AGGGGTCCAGT TGCGGCTTAT-3′

NBR2 no. T4-Reverse: 5′-TTCAGATCAAATGAAAACTTTTAC-3′

NBR2 no. T5-Forward: 5′-TAATACGACTCACTATAGGG AGGGGTCCAGT TGCGGCTTAT-3′

NBR2 no. T5-Reverse: 5′-CTTCCTGGGCTTCCAGCAC-3′

NBR2 no. T6-Forward: 5′-TAATACGACTCACTATAGGG AGGGGTCCAGT TGCGGCTTAT-3′

NBR2 no. T6-Reverse: 5′-AGGCCATTATCCTCAGCAAA-3′

Statistics and reproducibility. Most experiments were repeated 3–5 times to be eligible for the indicated statistical analyses, and the data exhibited normal distribution. There was no estimation of group variation before experiments. For gene expression and RIP assays, relative quantities of gene expression level were normalized. The relative quantities of RIP samples were normalized by individual inputs, respectively. All results are presented as mean ± the standard deviation (s.d.) of at least three independent experiments, unless otherwise noted. Each exact n value is indicated in the corresponding figure legend. Comparisons were performed using two-tailed paired Student's t-test ($^*P < 0.05$, $^{**}P < 0.01$, and $^{***}P < 0.001$), as indicated in the individual figures. For animal studies, five mice per group is the standard sample size for tumour xenograft experiments, and no statistical method was used to predetermine sample size. None of the samples/animals was excluded from the experiment, and the animals were not randomized. The investigators were not blinded to allocation during experiments and outcome assessment. For western blotting, representative images are shown. Each of these experiments was independently repeated 3–5 times. For survival analysis, the expression of *NBR2* was treated as a binary variant and divided into 'high' and 'low' level. Kaplan–Meier survival curves were compared using the Gehan–Breslow test with GraphPad Prism (GraphPad Software). The experiments were not randomized. The investigators were not blinded to allocation during experiments and outcome assessment.

36. Lee, S. W. *et al.* Skp2-dependent ubiquitination and activation of LKB1 is essential for cancer cell survival under energy stress. *Mol. Cell* **57,** 1022–1033 (2015).
37. Lin, A. *et al.* The FoxO-BNIP3 axis exerts a unique regulation of mTORC1 and cell survival under energy stress. *Oncogene* **33,** 3183–3194 (2014).
38. Gan, B. *et al.* Lkb1 regulates quiescence and metabolic homeostasis of haematopoietic stem cells. *Nature* **468,** 701–704 (2010).
39. Gan, B. *et al.* mTORC1-dependent and -independent regulation of stem cell renewal, differentiation, and mobilization. *Proc. Natl Acad. Sci. USA* **105,** 19384–19389 (2008).
40. Gan, B. *et al.* FoxOs enforce a progression checkpoint to constrain mTORC1-activated renal tumorigenesis. *Cancer Cell* **18,** 472–484 (2010).
41. Lin, A. *et al.* FoxO transcription factors promote AKT Ser473 phosphorylation and renal tumor growth in response to pharmacological inhibition of the PI3K-AKT pathway. *Cancer Res.* **74,** 1682–1693 (2014).
42. Gyorffy, B., Surowiak, P., Budczies, J. & Lanczky, A. Online survival analysis software to assess the prognostic value of biomarkers using transcriptomic data in non-small-cell lung cancer. *PLoS ONE* **8,** e82241 (2013).
43. Gyorffy, B. *et al.* An online survival analysis tool to rapidly assess the effect of 22,277 genes on breast cancer prognosis using microarray data of 1,809 patients. *Breast Cancer Res. Treat.* **123,** 725–731 (2010).

DOI: 10.1038/ncb3328

nature cell biology

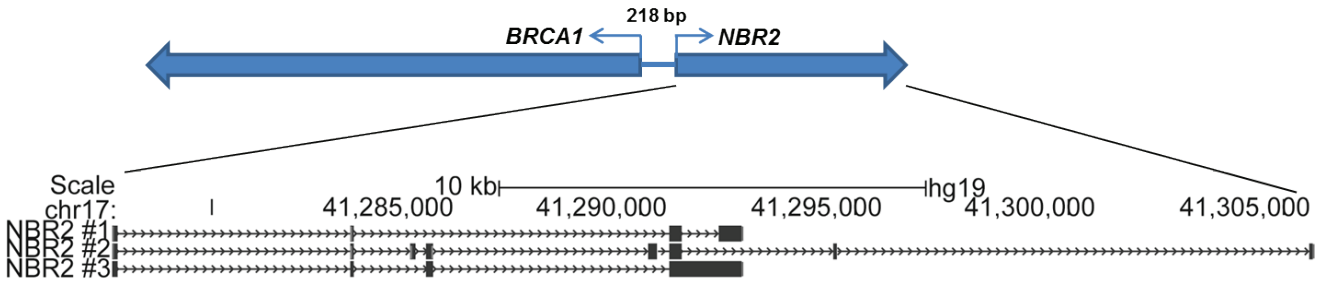

Supplemental Figure 1 The schematic diagram of the genomic region of human *BRCA1* and *NBR2* genes with different splicing isoforms**.** Arrows represent the direction of transcription.

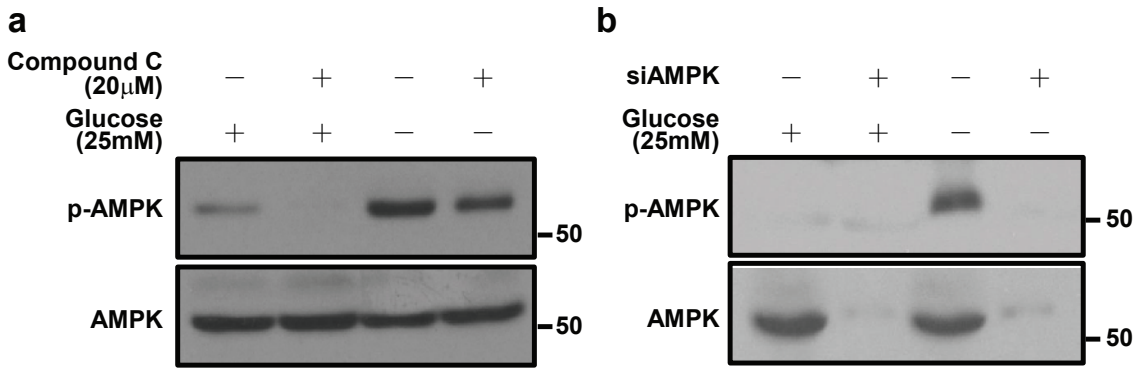

Supplemental Figure 2 AMPK inactivation by compound C or *AMPKα* siRNA treatment. **(a)** MDA-MB-231 cells were treated with 20 μM Compound C in 25 or 0 mM glucose-containing medium for 24 hours, and then subjected to Western blotting analysis to measure AMPK activation. **(b)** MDA-MB-231 cells transfected with *AMPKα* or control (Ctrl) siRNA were cultured in 25 or 0 mM glucose-containing medium for 24 hours, and then subjected to Western blotting analysis to measure AMPK activation. Unprocessed original scans of blots are shown in Supplemental Fig. 8.

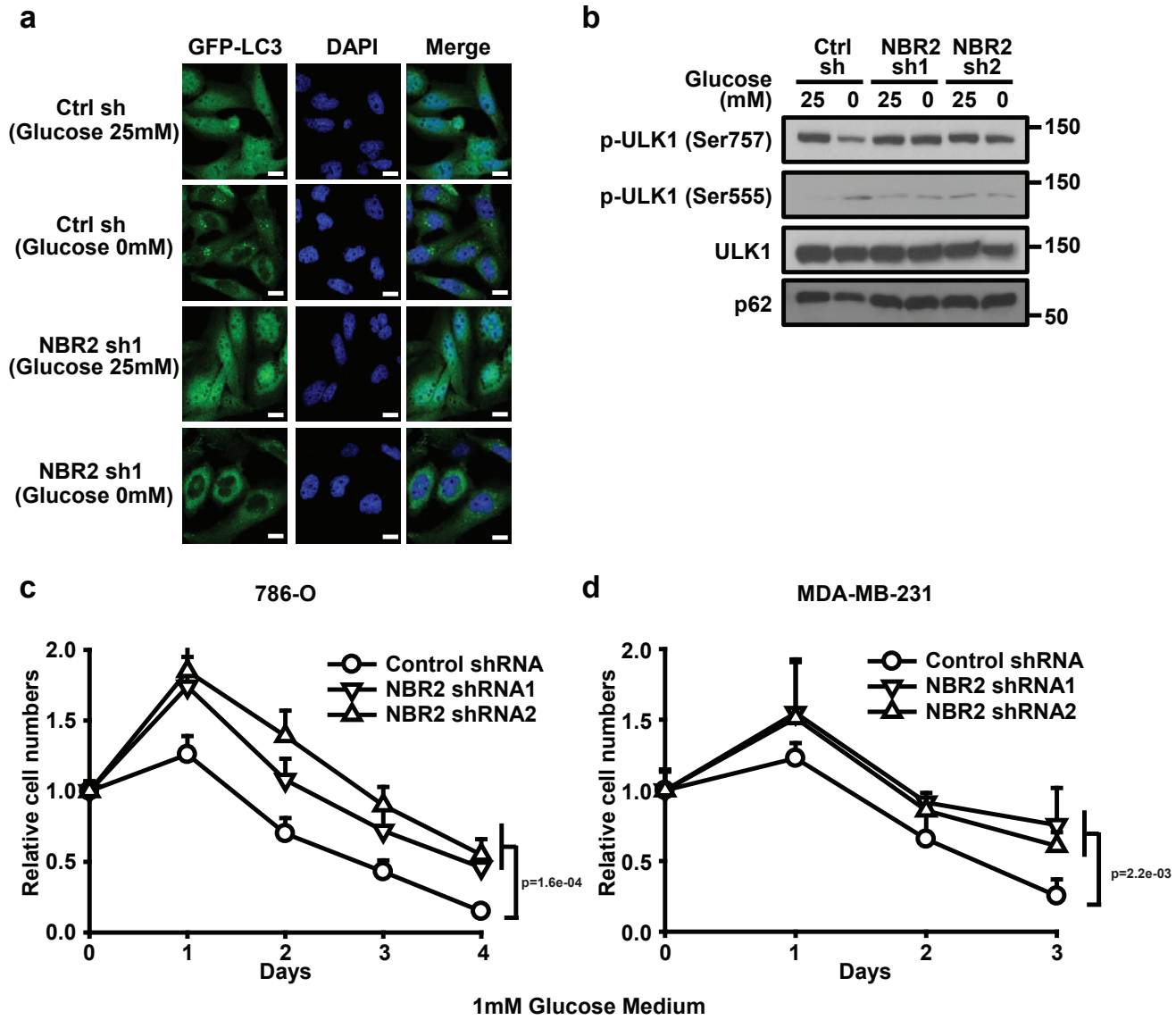

Supplemental Figure 3 *NBR2* knockdown affects autophagy and cell proliferation in response to energy stress. **(a)** The effect of *NBR2* deficiency on GFP-LC3 puncta formation. 786-O cells infected with either control shRNA or *NBR2* shRNA were transfected with GFP-LC3 plasmid, and then cultured in 25 or 0 mM glucose-containing medium for 18 hours. GFP-LC3 punctate foci were then detected using fluorescence microscopy. (Scale bars, 20 μm) **(b)** The effect of *NBR2* deficiency on ULK1 phosphorylation and p62 degradation in response to glucose starvation. MDA-MB-231 cells infected with either control shRNA or *NBR2* shRNA were cultured in 25 or 0 mM glucose-containing medium for 12h. Cell lysates were then analyzed by Western blotting. **(c, d)** Cells infected with either control shRNA or *NBR2* shRNA were cultured in 1mM glucose-containing medium for different days as indicated, and then subjected to cell proliferation analysis (Mean ± s.d., n=3 biologically independent extracts, two-tailed paired Student's t-test). Source data for c, d can be found in Supplementary Table 1. Unprocessed original scans of blots are shown in Supplemental Fig. 8.

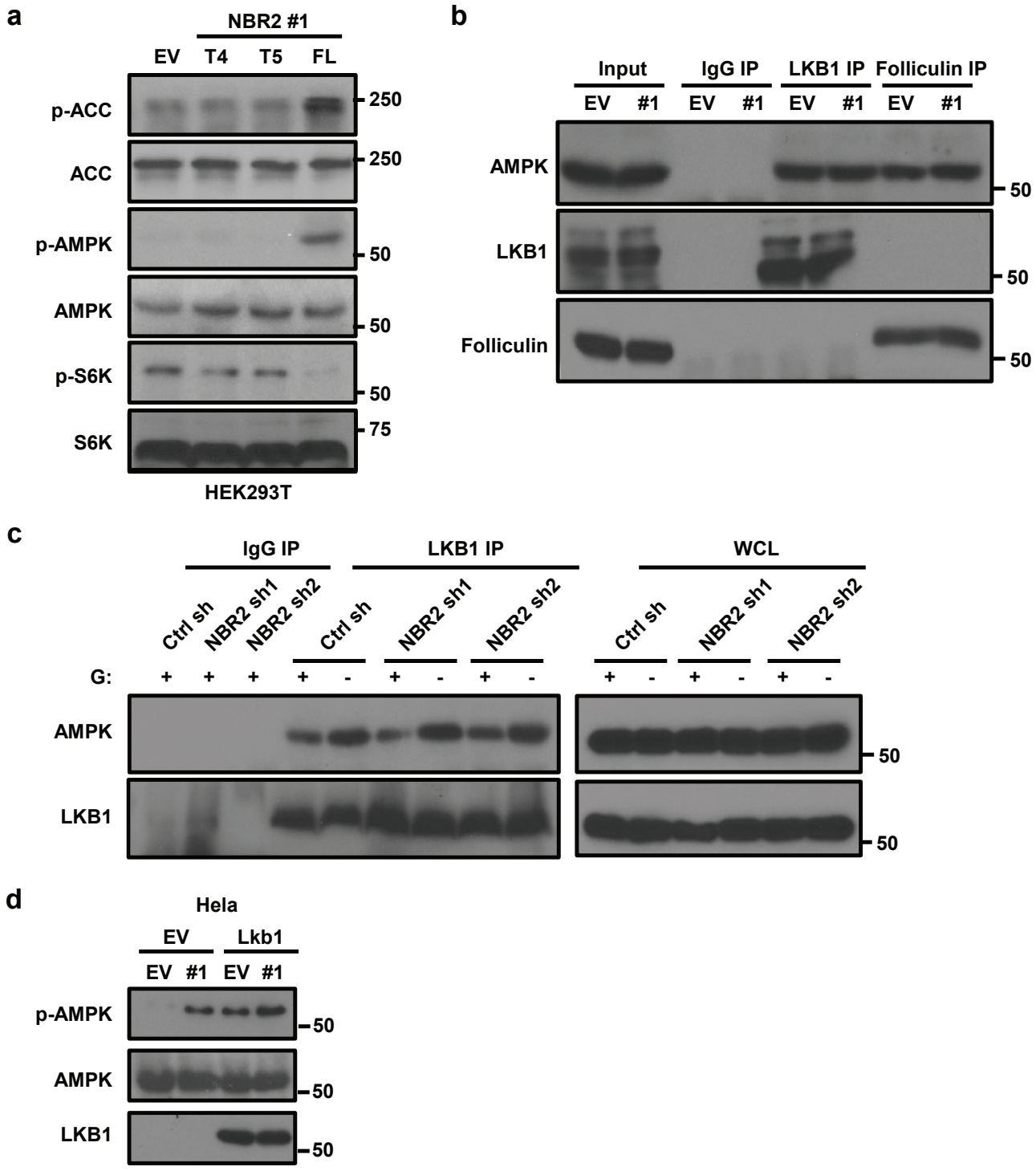

Supplemental Figure 4 Mechanistic studies of *NBR2* regulation of AMPK. **(a)** Protein lysates were prepared from HEK293T cells transfected with empty vector (EV), *NBR2* full length (FL), T4, or T5 fragment expression vectors, and analyzed by Western blotting as indicated. **(b)** Protein lysates prepared from UMRC2 cells stably expressing EV or *NBR2* #1 expression vectors were immunoprecipitated by IgG, LKB1 or Folliculin antibodies, and then were analyzed by Western blotting as indicated. Aliquots of the protein lysates (input) were also analyzed directly. **(c)** 786-O cells infected with either control shRNA or *NBR2* shRNA were cultured in medium containing 0 or 25 mM glucose for 12 hours. Protein lysates were prepared and immunoprecipitated by IgG or LKB1 antibodies, and then were analyzed by Western blotting as indicated. Aliquots of the protein lysates (input) were also analyzed directly. **(d)** Empty vector (EV) or LKB1-infected Hela cells were transfected with EV or *NBR2* #1 expression vectors. Protein lysates were prepared and analyzed by Western blotting as indicated. Unprocessed original scans of blots are shown in Supplemental Fig. 8.

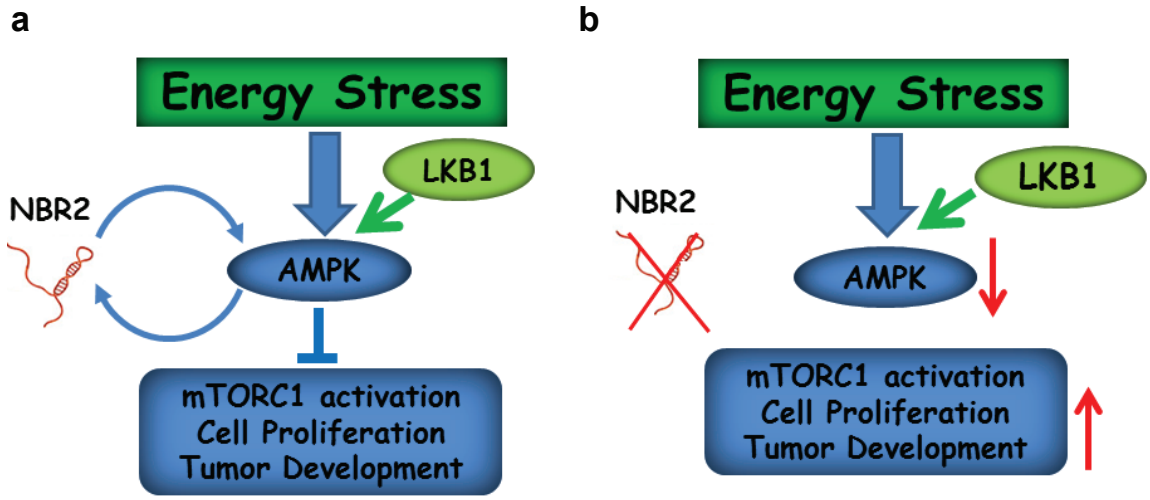

Supplemental Figure 5 The working model of the reciprocal regulation between *NBR2* and AMPK under energy stress, and its relevance to cancer development. See discussion for detailed description.

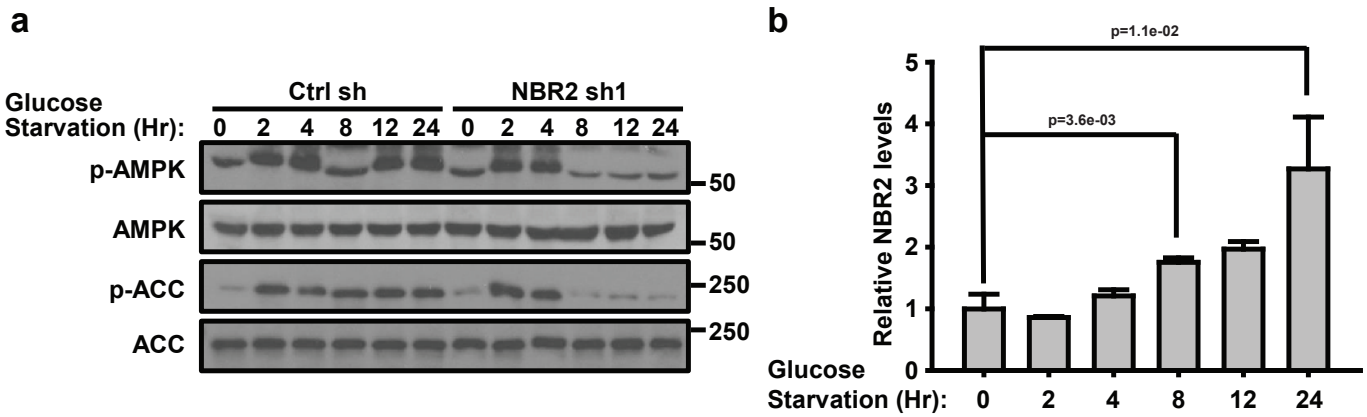

Supplemental Figure 6 *NBR2* deficiency affects AMPK activation under long periods of energy stress. **(a)** MDA-MB-231 cells infected with either control shRNA or *NBR2* shRNA were cultured in 0 mM glucose-containing medium for different hours, and protein lysates were prepared and analyzed by Western blotting**. (b)** MDA-MB-231 cells were cultured in 0 mM glucose-containing medium for different hours, and then subjected to real-time PCR analysis to measure *NBR2* expression (Mean ± s.d., n=3 biologically independent extracts, two-tailed paired Student's t-test). Source data for b can be found in Supplementary Table 1. Unprocessed original scans of blots are shown in Supplemental Fig. 8.

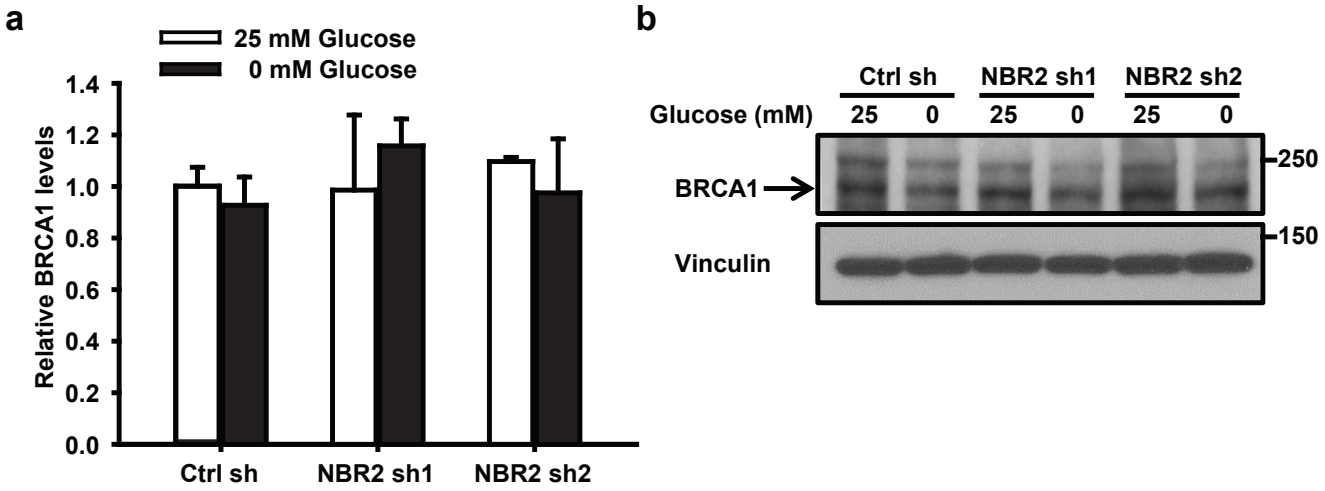

Supplemental Figure 7 *NBR2* deficiency does not affect *BRCA1* expression. **(a)** MDA-MB-231 cells infected with either control shRNA or *NBR2* shRNA were cultured in 25 or 0 mM glucose-containing medium for 24 hours, and then subjected to real-time PCR analysis to measure *BRCA1* expression (Mean ± s.d., n=3 biologically independent extracts, two-tailed paired Student's t-test). **(b)** Cell lysates were also analyzed by Western blotting as indicated. Source data for a can be found in Supplementary Table 1. Unprocessed original scans of blots are shown in Supplemental Fig. 8.

Fig. 1d

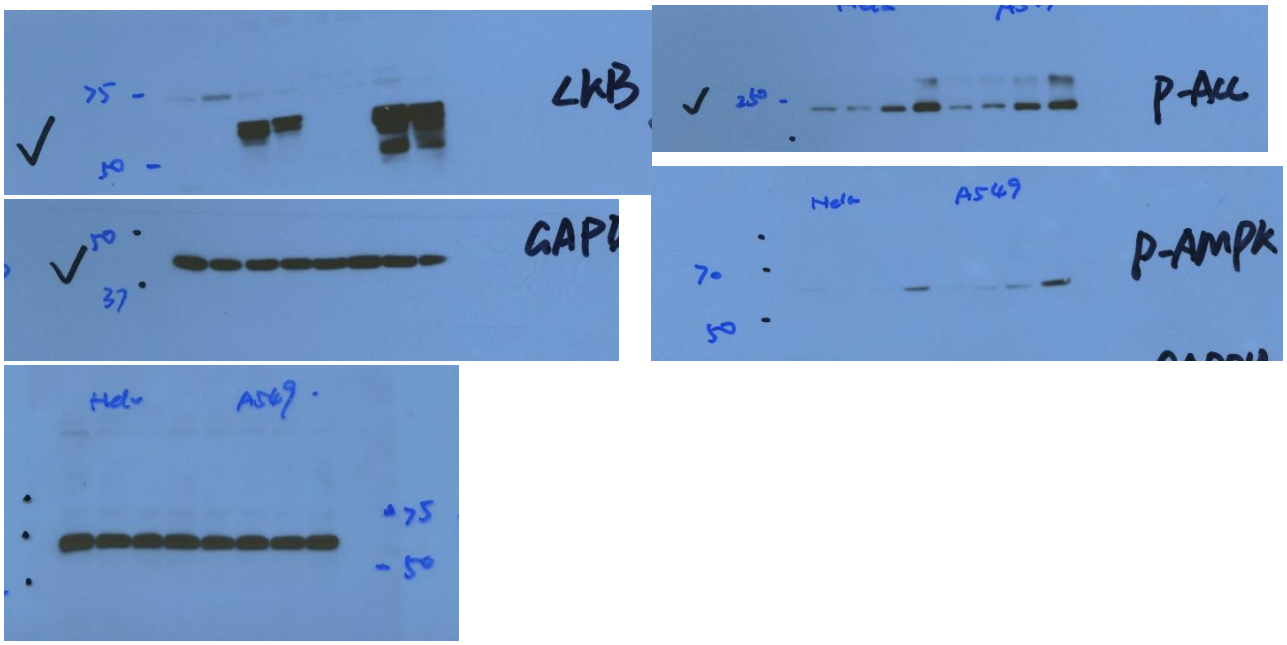

Supplemental Figure 8 Unprocessed scans of full blots.

Fig. 2 b

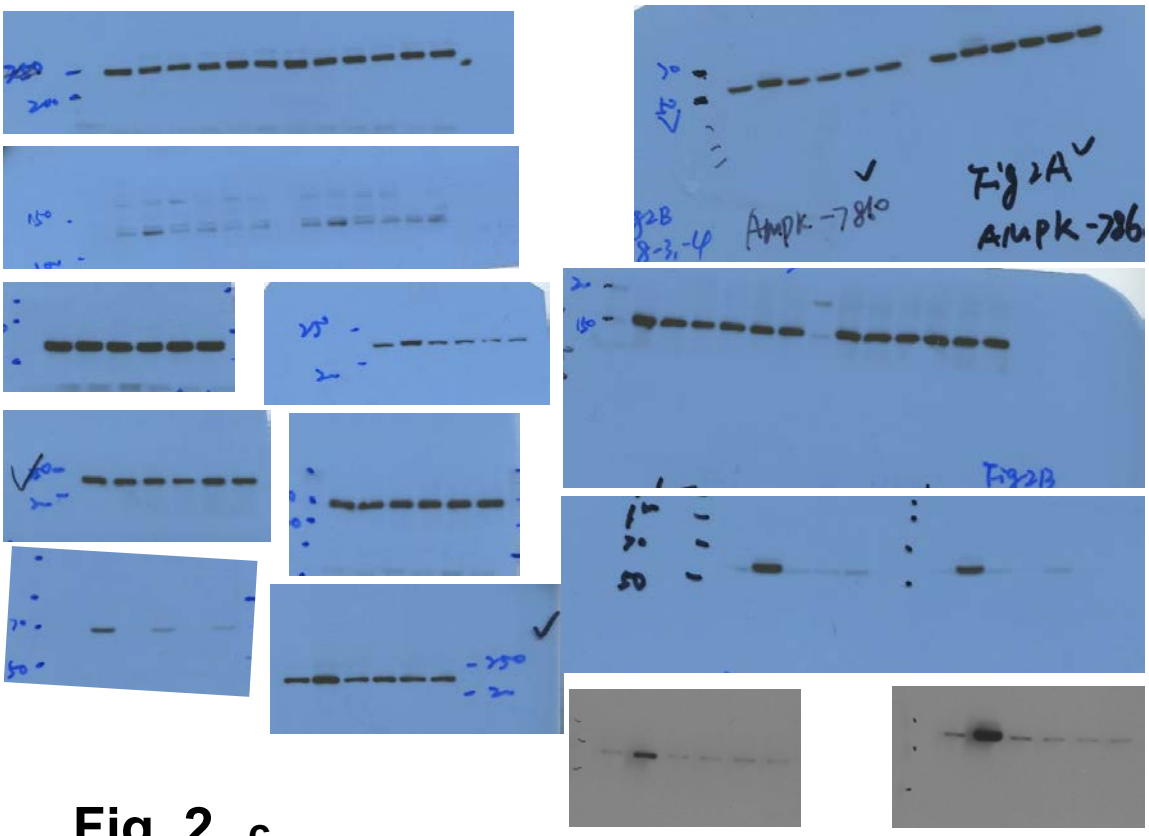

Fig. 2 c

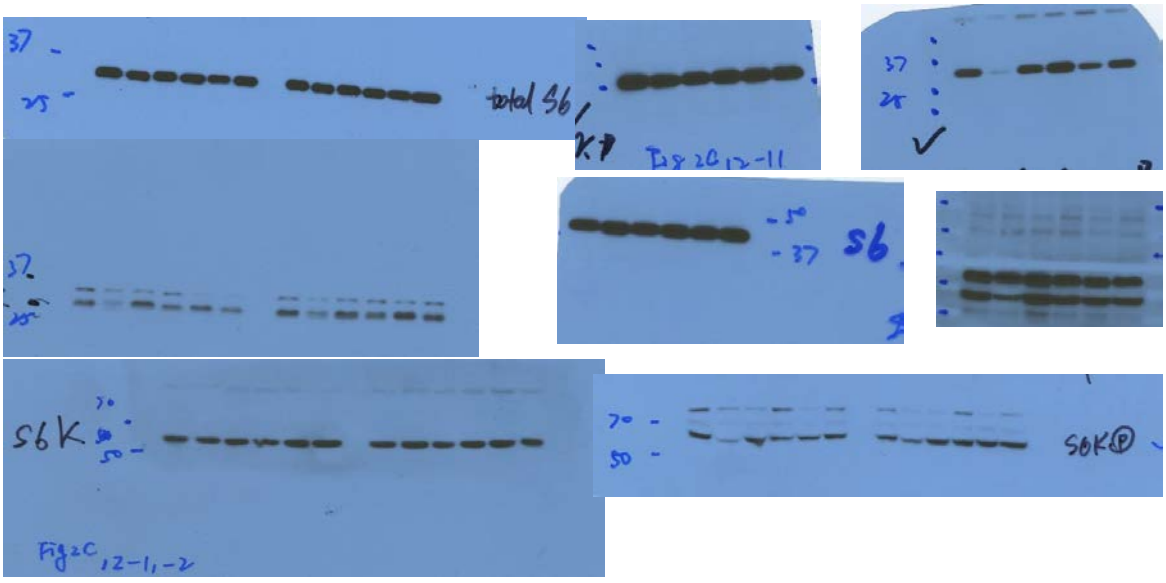

Supplemental Figure 8 continued

Fig. 2 d

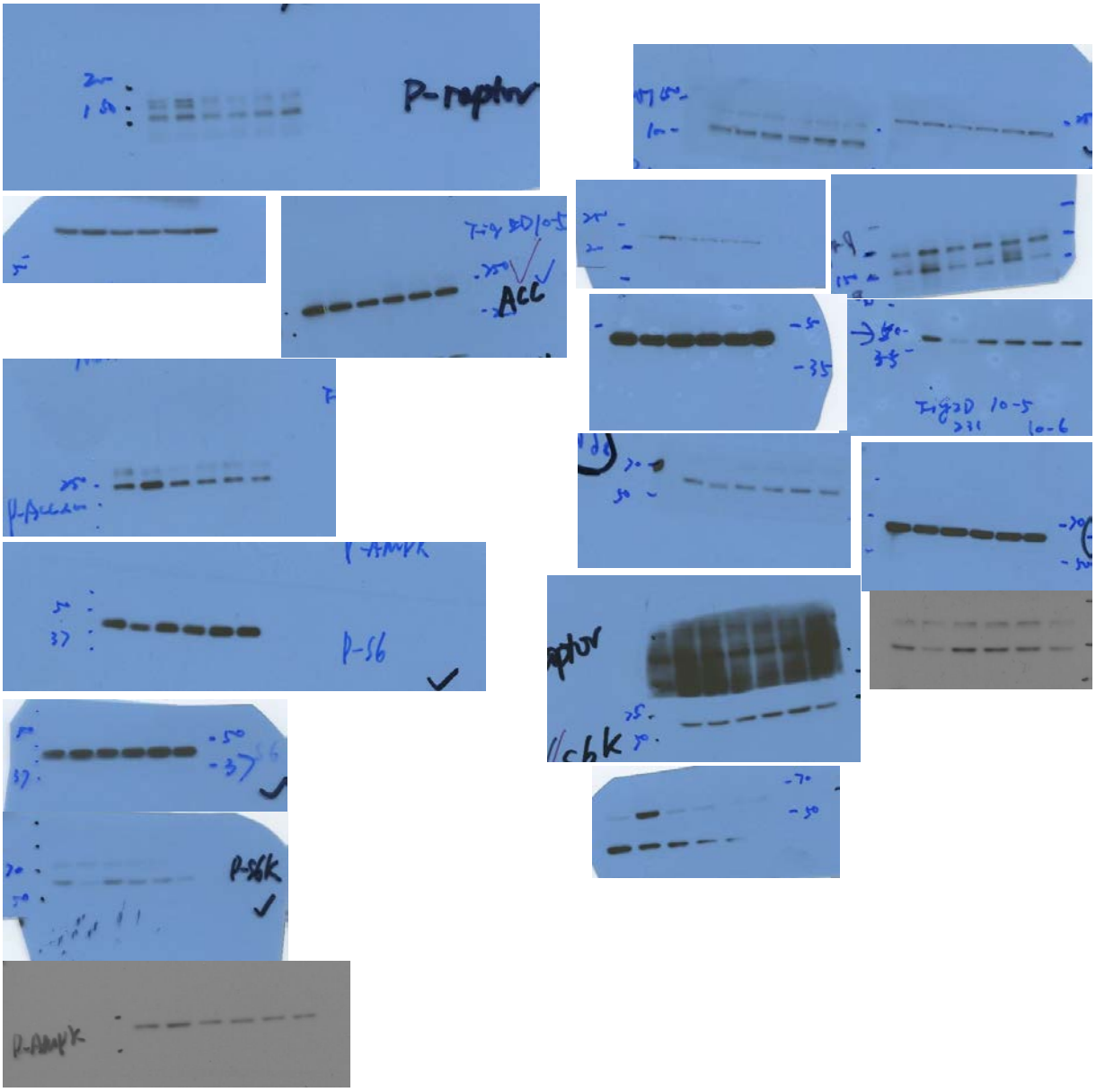

Fig. 2 e

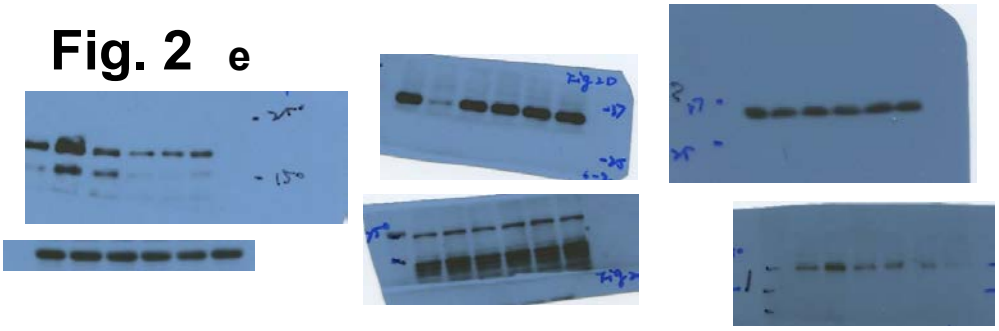

Supplemental Figure 8 continued

Fig. 3f

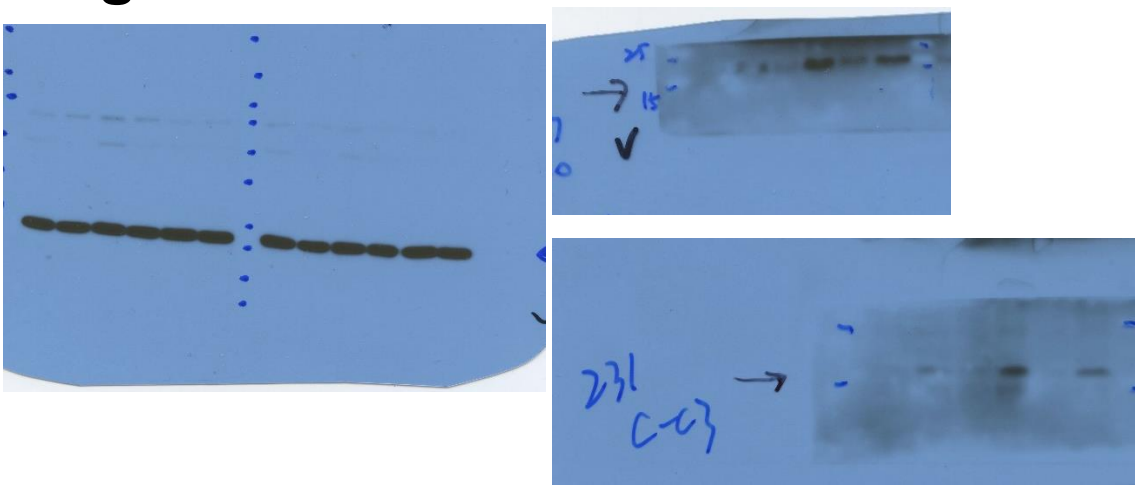

Fig. 4d

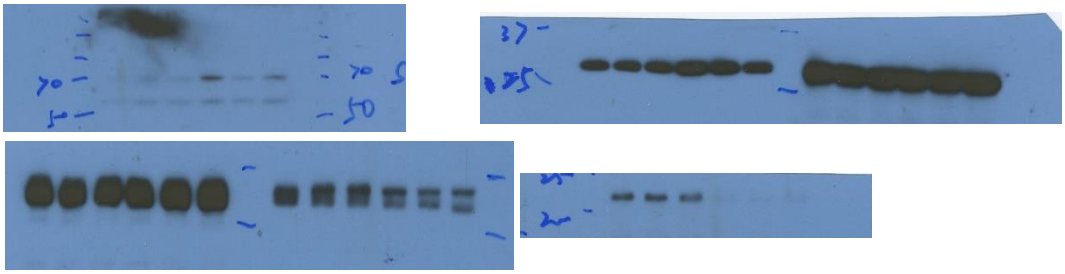

Supplemental Figure 8 continued

Fig. 5

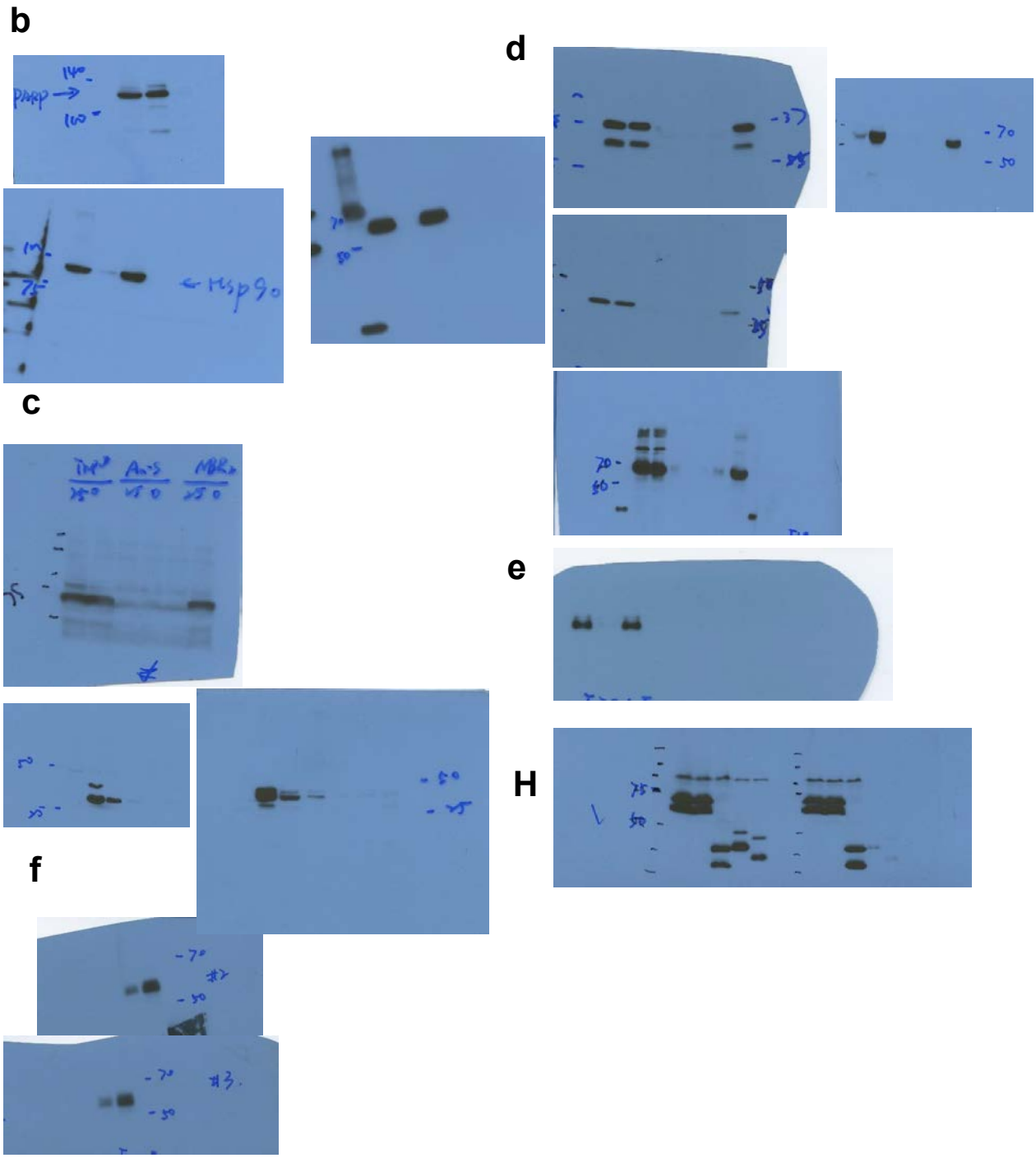

Supplemental Figure 8 continued

Fig. 6

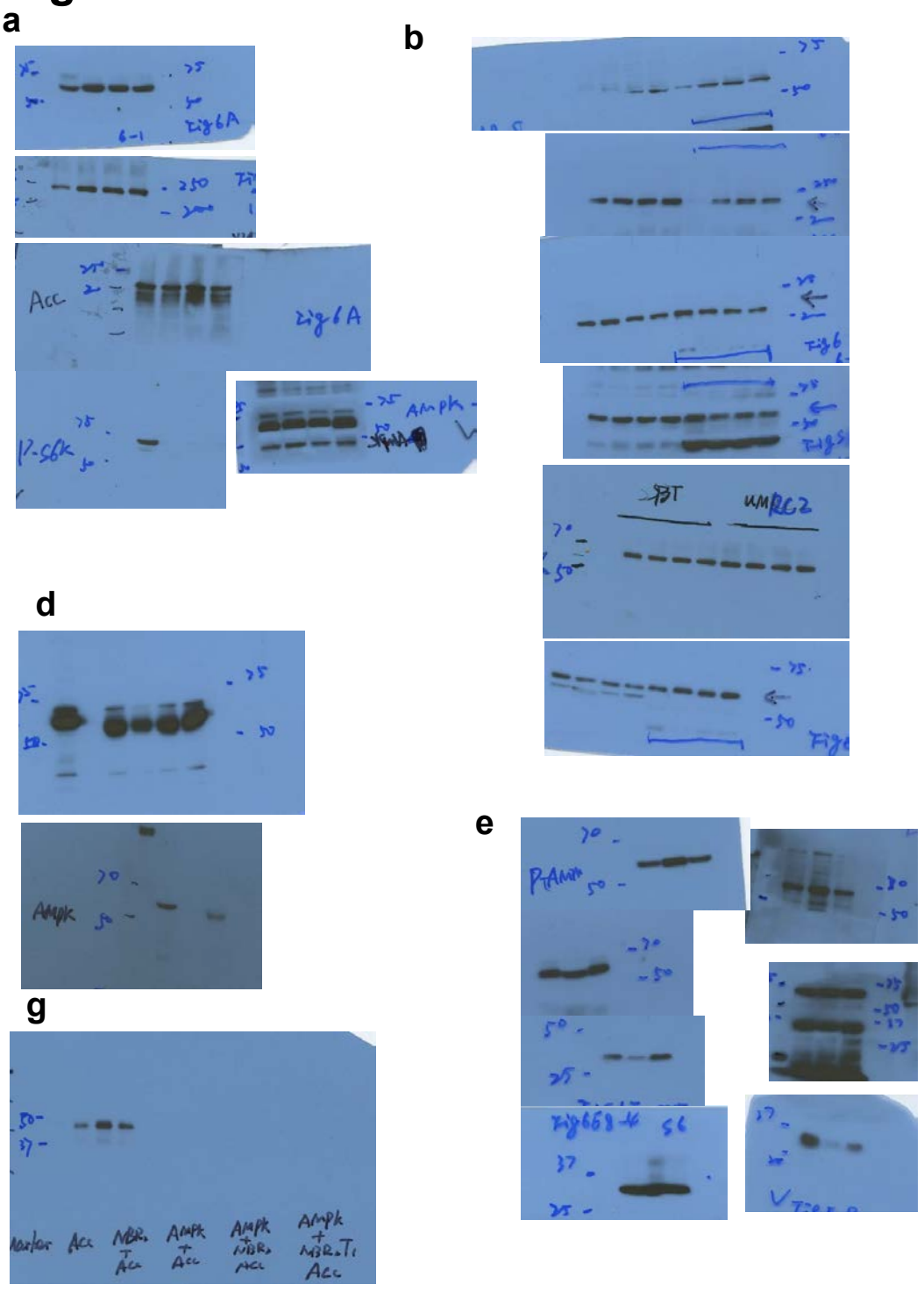

Supplemental Figure 8 continued

Fig. 7

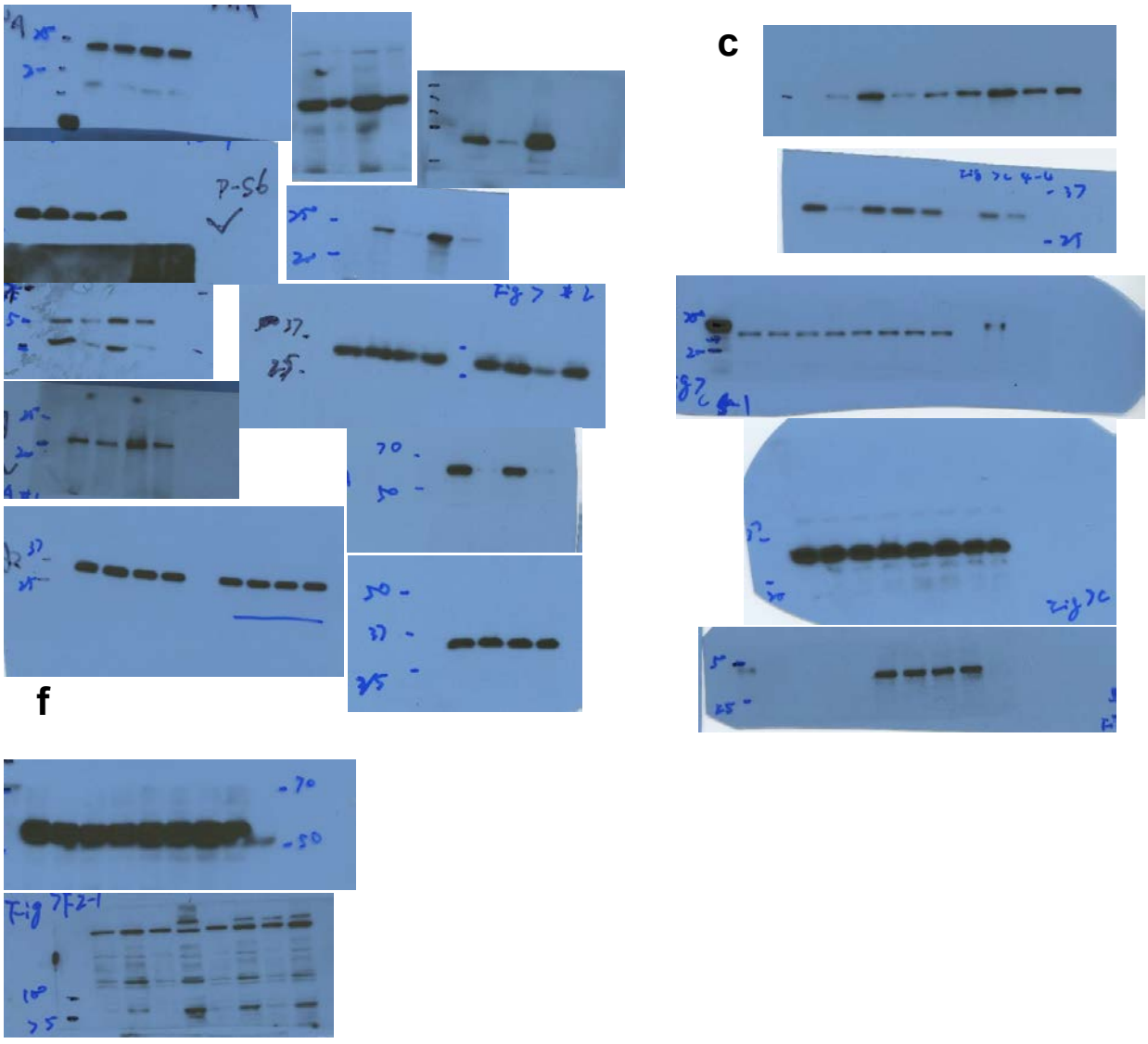

Supplemental Figure 8 continued

Fig. S2

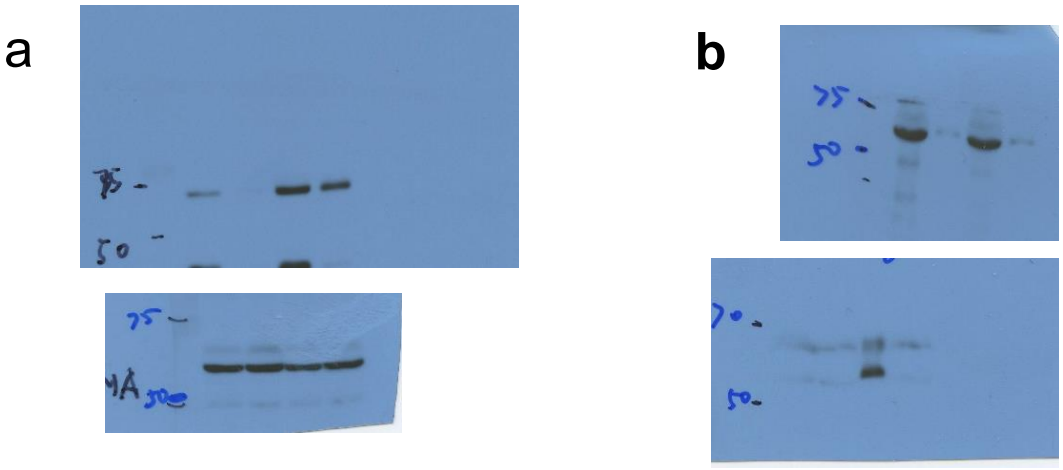

Fig. S3 b

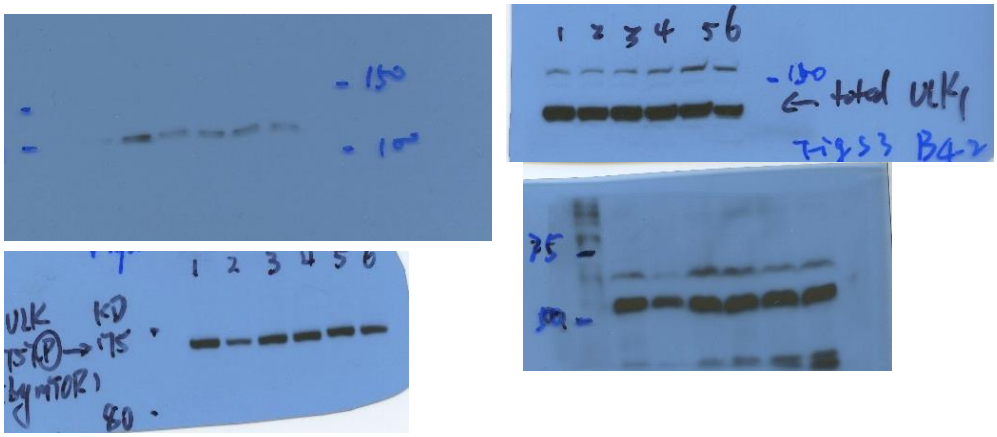

Supplemental Figure 8 continued

Fig. S4

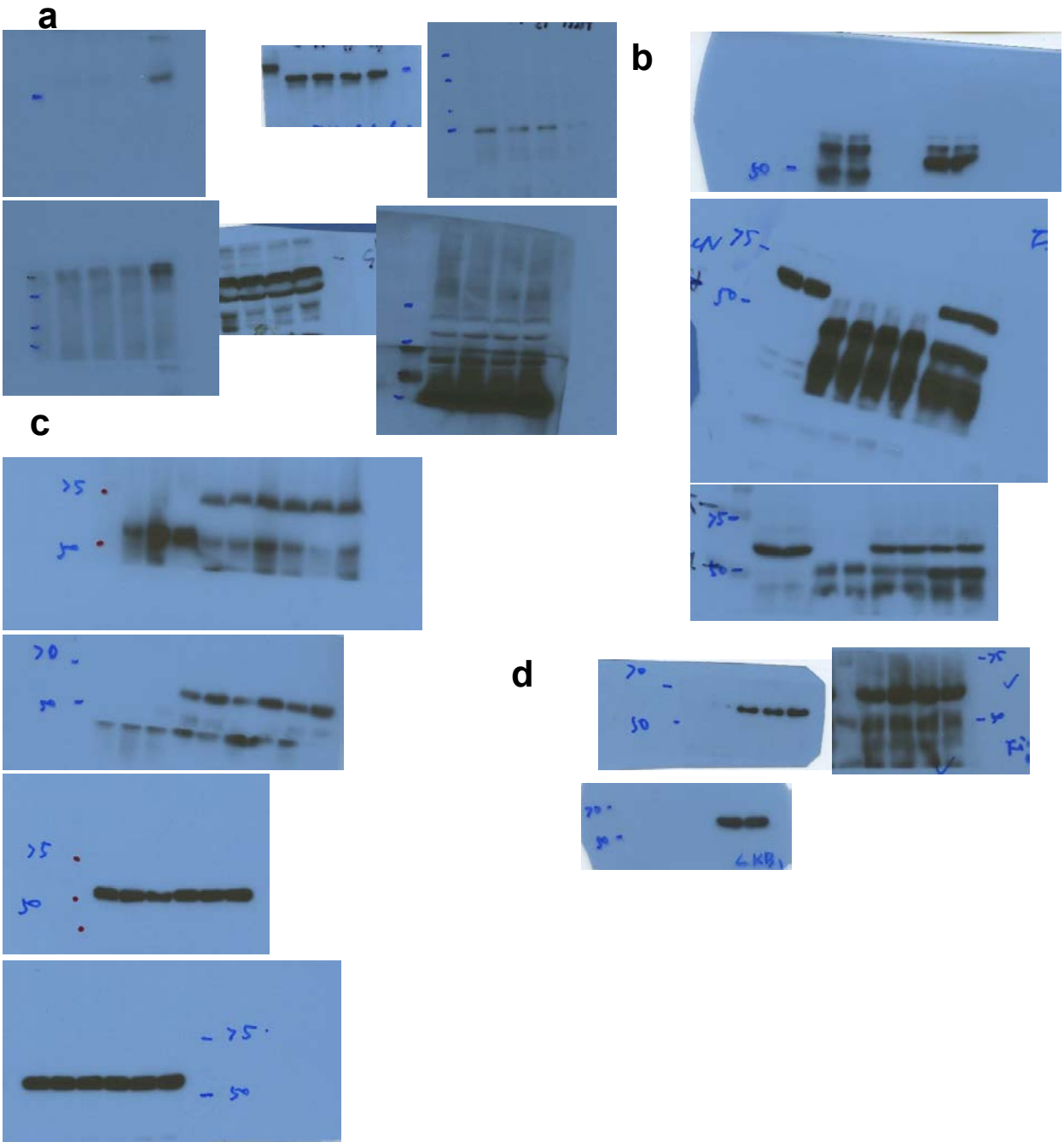

Supplemental Figure 8 continued

Fig. S6

a

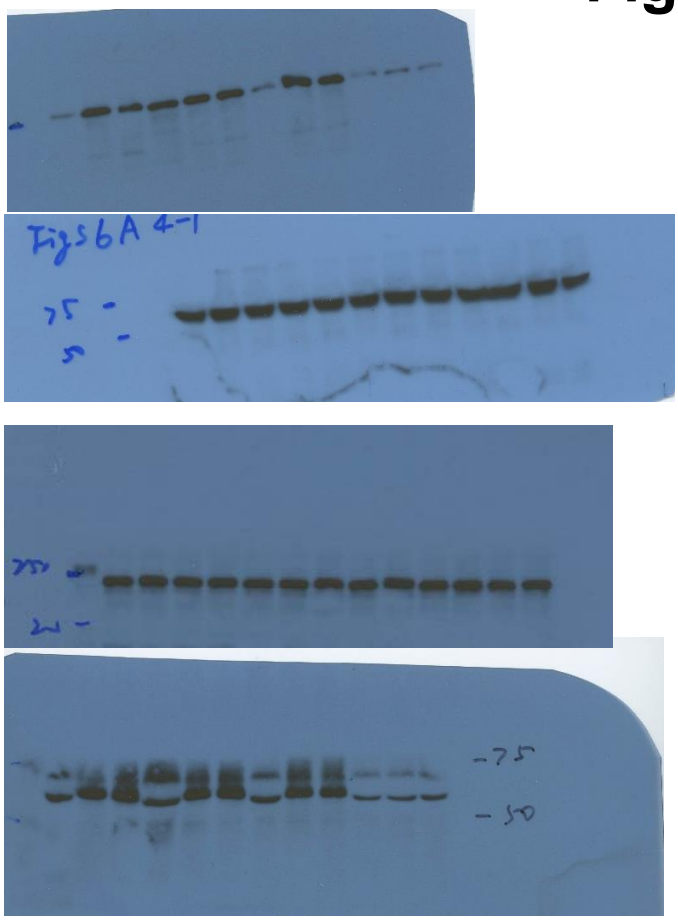

Fig. S7

b

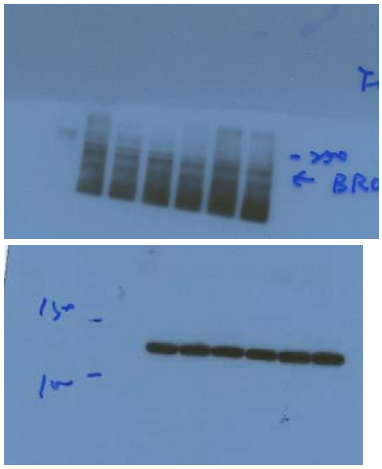

Supplemental Figure 8 continued

Supplementary Table 1 Statistics source data.
Raw numbers (cell number) or normalized values of the indicated figure panels are provided.